Translational and Rotational Motion of Disk-Shaped Marangoni Surfers

Samrat Sur[1], Hassan Masoud[2], and Jonathan P. Rothstein[1*]

[1] Department of Mechanical Engineering, University of Massachusetts, Amherst, MA 01003, USA

[2] Department of Mechanical Engineering- Engineering Mechanics, Michigan Technological University, Houghton, Michigan 49931, USA

[*]rothstein@ecs.umass.edu

Abstract

In this paper, we study the Marangoni propulsion of a neutrally buoyant disk-shaped object at the air-water interface. Self-propulsion was achieved by coating the back of the disk with either soap or isopropyl alcohol in order to generate and then maintain a surface tension gradient across the surfer. As the propulsion strength and the resulting disk velocity were increased, a transition from a straight-line translational motion to a rotational motion was observed. Although spinning has been observed before for asymmetric objects, these are the first observations of spinning of a geometrically axisymmetric Marangoni surfer. Particle tracking and Particle Image Velocimetry (PIV) measurements were used to interrogate the resulting flow field and understand the origin of the rotational motion of the disk. These measurements showed that as the Reynolds number was increased, interfacial vortices attached to sides of the disk were formed and intensified. Beyond a critical Reynolds number of $Re > 120$, a vortex was observed to shed resulting in an unbalanced torque on the disk that caused it to rotate. The interaction between the disk and the confining wall of the Petri dish was also studied. Upon approaching the bounding wall, a transition from straight-line motion to rotational motion was observed at significantly lower Reynolds numbers than on an unconfined interface. Interfacial curvature was found to either enhance or eliminate rotational motion depending on whether the curvature was repulsive (concave) or attractive (convex).

1. Introduction

Marangoni flows are induced by a gradient in interfacial tension resulting from a local variation of composition or temperature [1]. In the past, Marangoni effect has been used for propulsion of small objects attached to a fluid-fluid interface. In biological systems, self-induced Marangoni propulsion has been observed in organisms ranging in size from bacteria to water-walking insects. For example, surface-associated bacteria such as *Pseudomonas aeruginosa* have been shown to use signaling molecules exuded from their bodies to reduce the local surface tension. They have been observed to use the resulting Marangoni flow to rapidly migrate across the air-water interface towards nutrient-rich regions ripe for colonization [2, 3]. In the case of water-walking insects like Dianous (rove beetle) and Velia (small water strider), these insects have been shown to secrete surface-active materials to boost their water walking speed in emergency situations [4-7].

In the case of man-made objects, perhaps the most ubiquitous example of Marangoni propulsion is the camphor boat [8-10]. Suematsu et al. [9] investigated the motion of a camphor boat by placing a disk of camphor underneath a small boat to produce a low surface tension region behind the boat and propel the boat forward. They observed a number of different propulsion modes including continuous, intermittent or oscillatory motion depending on the placement location of the camphor disk on the boat. They explained these different modes as being the result of differences in the diffusion length of the camphor from beneath the boat to the air water interface. Renney et al. [10] investigated the Marangoni propulsion of a series of different shaped boats using a number of low-surface-tension water-miscible solutions to induce surface tension gradients. Their investigations showed that geometrically symmetric boat designs tended to move with a straight-line motion while asymmetries in the design of the boat could be used to induce rotational motion of the boat. Rotation of other geometrically asymmetric particles has been commonly observed in the literature. Nakata et al. [11] showed through experimental studies on camphor scrapings that the direction of rotational motion is governed by the shape and asymmetry of the particle. In some cases, the geometric asymmetry was specifically designed to maximize rotation rate to create interfacial Marangoni

rotors [12]. Takabatake et al [13] experimentally investigated the motion of a solid/liquid composite, a droplet of an oleic acid with a solid cylinder of sodium oleate attached to one side. They observed that the mode of motion of the solid/liquid composite dependents on the relative size of the solid with respect to that of the liquid. As the size of the solid was increased, the mode of motion switched from a spinning motion to a translational motion and then to an orbital motion. Nagai et al [14] further extended the work of Takabatake et al [13] numerically by using Stokes equation to solve for the flow field around the droplet. They observed that advective non-linearity caused symmetry break which led to rotational motion and that rotational motion of the droplet was a function of the droplet size. Recent experiments by Gidituri et al [15] on a fully wetted ellipsoid demonstrated that, at low enough Reynolds numbers, any rotational motion is weak and any perturbation to the flow field will damp out thus resulting in a swimmer that follows a purely translational motion. Finally, Soh et al.[16, 17], both numerically and experimentally, explored the hydrodynamic interactions in an ensemble of millimeter-sized camphor-releasing gel particles. They demonstrated that such interactions derive the self-assembly of the surfers and can be regulated via adjusting the shape of the particles.

Surface tension driven motion of interface-bound particles has been investigated theoretically as well. For instance, Lauga and Davis [18] analytically calculated the propulsion speed of an active disk in the absence of inertia. The derivations involve simultaneously solving for the Stokes and Laplace equations for, respectively, the flow of the liquid and the transport of the released chemical species. The calculations showed that the translational propulsion speed is independent of the size of the disk. A similar study was also carried out by Würger for a spherical particle [19]. Masoud and Stone [20] used the reciprocal theorem to derive closed-from expressions for the propulsion speed of chemically active oblate and prolate spheroids. Employing a Fourier spectral method, Masoud and Shelley [21] examined the collective surfing of many interface-trapped active particles. More recently, Vandadi et al. [22] theoretically examined the motion of chemically and thermally active particles in the presence of a confining solid wall located below the liquid-gas interface. Their analytical calculations revealed that the particles may propel in the lower

surface tension direction depending on their geometry and the thickness of the liquid layer sandwiched between the interface and the wall.

Even in the absence of Marangoni propulsion, objects floating on an air-water interface can spontaneously move because of interfacial curvature. For a dense particle, with a large contact angle, floating on the surface of a liquid, the weight of the particle can deform the fluid interface downward. On a flat interface devoid of other particles, interfacial curvature alone will not result in particle motion. However, the presence of a second dense particle or a wall around which a similar interfacial curvature exists will result in an attractive force between the particles that scales like the inverse of their separation and will result in spontaneous particle motion [23]. This is because for two objects that have like (concave or convex) curvature around them, both the gravitation potential energy and the capillary energy will decrease as the objects approach each other [23]. This attractive force can result in the self-assembly of floating objects into particle rafts [24-28] or the accumulation of particles near regions of high interfacial curvature [29, 30].

In this study, we investigated the motion of a self-propelled axisymmetric Marangoni surfers in order to understand the role of propulsion strength, Reynolds number and interface curvature on its motion and the details of the flow around it. In these experiments, a cylindrical disk was propelled either by a solution of isopropyl alcohol (IPA) or a commercially-available soap. The motion of the disk was optically tracked while the details of the fluid dynamics were probed using Particle Image Velocimetry (PIV). At low speeds and low Reynolds numbers, the disks were observed to move in a straight line. However, disks moving at higher speeds, above a critical Reynolds number, were observed to spontaneously rotate. Through PIV measurements, this rotational motion was found to be directly linked to the shedding of an attached vortex. Under the right conditions, the presence of a confining boundary wall with and without interface curvature was also found to result in particle rotation, although at a significantly lower Reynolds number. These studies are the first to show that a transition from linear to rotational motion can exist for a self-propelled Marangoni surfer even if the surfer is geometrically axisymmetric.

2. Experimental Setup

Experiments were performed in a large and small Petri dish of diameter D=150mm and D=86mm as shown in Figure 1. The depth of water was maintained at h=50mm in the large Petri dish and at h=12mm in the small Petri dish. In both cases, the motion of the Marangoni surfers was found to be insensitive to the depth of the water in the Petri dish. All the experiments were performed in the large Petri dish except for the experiments where the effect of the boundary wall on the mode of motion of the Marangoni surfer was probed. Isopropyl alcohol (IPA) and commercially available soap (Dawn) were used to induce the gradient in surface tension needed to produce the desired Marangoni flow. A thin film of either soap or IPA was applied to the disk by dip coating 1mm of the 4mm disk into a liquid bath resulting in the coating shown schematically in Figure 1d. A number of different strength solutions of IPA and water solutions

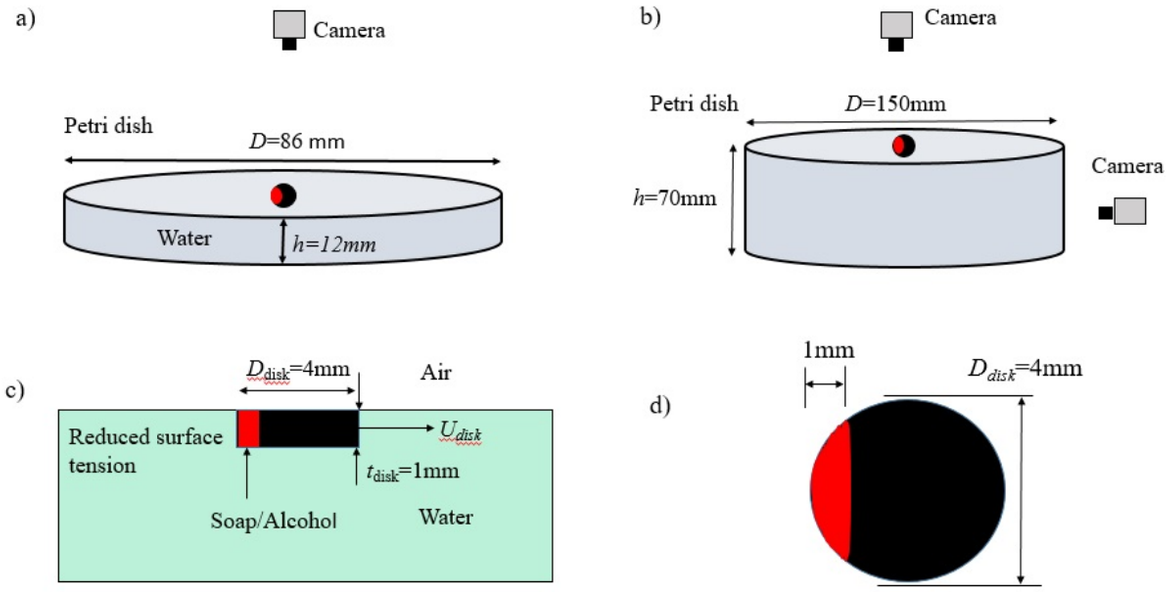

Figure 1. A schematic of the experimental setup of a a) small and a b) large Petri dish. The diameter of the small Petri dish was D=86mm and the large Petri dish was D=150mm. The depth of water in the small Petri dish was maintained at h=12mm and in the large Petri dish it was maintained at h=50mm. Two different optical setups were used for recording as shown in a) and b). Side view of the D_{disk}=4mm and t_{disk}=1mm cylindrical disk is shown in c). d) Top view of the disk showing the region where soap/alcohol was applied. The disk is propelled by soap/alcohol released from the back of the disk in the area denoted in the red region.

were used in order to modify the propulsion strength. In all cases, the soap film was a mixture of 50% soap and water. This dip coating process resulted in the deposition of approximately 1mg of the propulsion agent in the back of the disk in each case. The surface tension of pure IPA was taken from literature to be σ = 22mN/m, while the surfactant in the Dawn soap is known to reduce the interfacial tension of water from σ = 72mN/m to 30mN/m [31]. The concentration of the soap used was above the critical micellar concentration. The cylindrical disk had a diameter of D_{disk}=4mm and a thickness of t_{disk}=1mm. The disks were fabricated from polydimethylsiloxane (PDMS) which has a density of ρ=965Kg/m^3. A close optical inspection of the interface around the floating disk showed a flat interface.

The disks were placed on to the air-water interface and released using a mechanical stage to ensure a reproducible release protocol. The disks were initially balanced on the top of a post measuring 30mm tall with a diameter of 3mm. The post was connected to a stepper motor through a thin cantilever fully submersed in the water. To deposit the disk, the post was driven down at a velocity of 10mm/s and submersed to a depth of 3mm below the water's interface. As a result, from initial touchdown to release of the disk, the disk was held stationary by the post for 0.1s before it was allowed to move freely. A digital

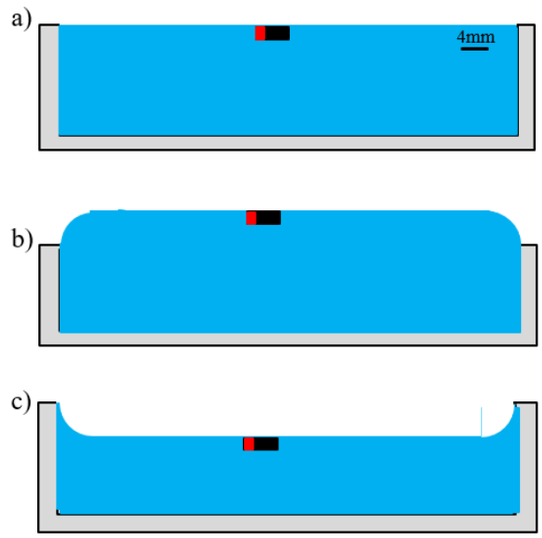

Figure 2. A schematic of interface curvature at the boundary of a D=86mm Petri dish showing a) a flat b) a convex and c) a concave interface.

camera was used to track the motion of the swimmer. The videos were captured at 17fps and the images were fed into a particle tracking software (Tracker) which was used to analyze the motion of the particles. For the Particle Image Velocimetry (PIV) measurements, a 300mW argon ion laser was used to create a laser light sheet and illuminate 40μm PIV particles dispersed in the water and captured using a high-speed video camera. PIV measurements were used to analyze the flow field induced by Marangoni flow along the air-water interface and underneath the disk. The PIV videos were analyzed using a commercial PIV software (LaVision).

In order to study the effect of confinement and the role that interface curvature can play on the motion of the disk, the small Petri dish was used. At the edge of the Petri dish, a concave, convex, or a flat interface was created by first filling dish with water until the contact line was pinned to the top edge of the Petri dish as shown in Figure 2. Once the contact line was pinned, a syringe pump was then used to either add or withdraw 9ml of water to produce the desired curvature of the air-water interface.

3. Results and Discussions

3.1 Motion of an Disk-Shaped Interfacial Swimmer Propelled by Soap

In this section, the motion of the disk-shaped Marangoni swimmer that uses soap as the propulsion agent is presented. As described in section 2, a solution of 50% soap and water was used to coat the back of the disk. Upon deposition of the disk onto the air-water interface, the surfactants in the soap quickly began to dissolve in the water and to populate the air-water interface reducing its interfacial tension towards σ=30mN/m which is the interfacial tension value if the water interface is fully saturated with surfactant. The minimum surface tension will arise very near to the region of the disk coated by the soap where the surfactant concentration at the interface is the largest. The resulting gradient in surface tension drives a Marangoni flow in the liquid and propels the disk in the direction of higher surface tension. At a steady state velocity, the capillary forces on the disk, which are calculated by integrating the surface tension along the contact line between the disk and the water, are balanced by the hydrodynamic drag force.

When soap was used as the propulsion agent, a linear, straight-line translation of the disk was observed. As seen in Figure 3 for a representational case of the 50wt% soap-water solution, the disk initially accelerated upon release before reaching a maximum velocity of roughly U_{disk}=14mm/s after a time of t=0.7s. This translates to a maximum Reynolds number of, $Re = \rho U_{disk} D_{disk} / \mu = 60$ where, ρ is the density of the fluid, U_{disk} is the maximum velocity of the disk, D_{disk} is the diameter of the disk and μ is the viscosity of the water. During the initial start-up of motion, the acceleration was found to remain roughly constant at a=25mm/s^2. Beyond the peak velocity, the disk was found to decelerate slowly before reaching a steady-state velocity of U_{disk}=4mm/s (Re=16) approximately t=5s after the disk was released. This steady state motion was observed for at least 30 seconds or until the disk collided with the wall of the Petri dish. These observations suggest that, at long times, a constant release rate of the soap from the disk to the air-water interface was achieved. Given the 1mg of the soap solution was used in the coating, the average release rate of soap from the disk becomes 0.03mg/s.

Multiple experiments were performed using soap as the propulsion agent to determine an average maximum and steady-state velocity. For the case of 50wt% soap-water solution the average maximum velocity was U_{disk}=16$\pm$2mm/s and the average steady state velocity was U_{disk}=5.0$\pm$0.6mm/s. As the concentration of soap was reduced to 25wt%, the maximum velocity dropped to U_{disk}=8.3$\pm$0.9mm/s and the steady state velocity reduced to U_{disk}=2.0$\pm$0.6mm/s. Thus, the velocity of the disks is roughly linearly dependent on the concentration of the soap in the solution used to dip coat the disks and therefore the rate of release of the surfactant from the surface of the disk into the surrounding water. This will be seen again in the sections that follow when IPA is use as the propulsion agent. It is also important to note that the duration of the observed steady-state motion was a function of the quantity of propulsion agent applied to the disk as well as the rate at which the propulsion agent dissolved into the water.

Finally, it is important to note that, in these experiments, the variations in the surfactant concentration field is dominated by convection of the induced Marangoni flow and not the diffusion of the surfactant molecules across streamlines. This can be demonstrated by calculating the Peclét number, Pe =

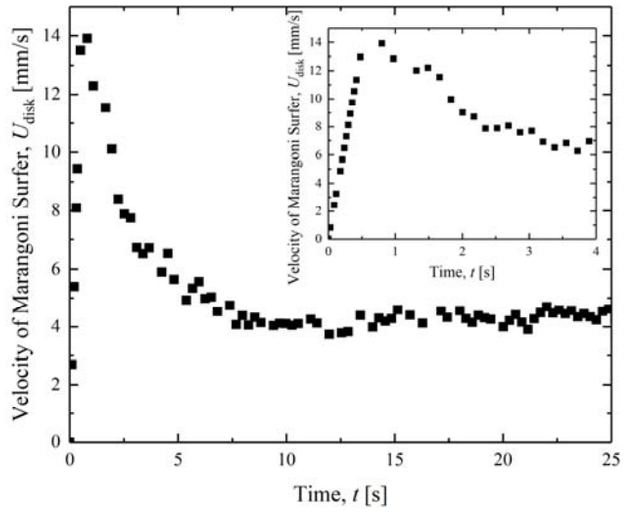

Figure 3. Plot of disk velocity, $U_{disk,}$ as a function of time, t, for the Marangoni swimmer using surfactant as the propulsion agent. Inset shows close up of data at early times.

$D_{disk}U_{disk}/D$, which compares the relative importance of convection to diffusion. The appropriate length scale to use for the Peclét number in this case is the diameter of the disk, D_{disk}, U_{disk} is the velocity of the disk and D is the diffusion coefficient of the surfactant in water. Given that the diffusion coefficients for the two surfactants in the soap, sodium laureth sulfate and sodium lauryl sulfate, are on the order of $D \sim 0.5\text{x}10^{-9}$ m^2/s, the resulting Peclét number in these experiments becomes extremely large, $Pe \sim 10^5$.

3.2 PIV of the Flow Field Around a Disk-Shaped Interfacial Swimmer Propelled by Soap

In this section, Particle Image Velocimetry (PIV) measurements of the flow field along the air-water interface and underneath a disk-shaped Marangoni swimmer propelled by soap are presented after the disk has achieved a steady state velocity. In Figure 4a and 4b, PIV measurements of the interfacial flows around the disk is shown for the disk undergoing a constant velocity translational motion as shown in the final 20s of data in Figure 3. In Figure 4, the disk motion is from left to right. As seen in Figure 4a, the interface appears to dilate, spreading radially from a stagnation point roughly one diameter downstream of the trailing edge of the disk. The stagnation point in the PIV data represents the location of the minimum in the interfacial tension. It is from the trailing edge of the disk that the surfactant is released and where the interfacial tension is minimized. The presence of a stagnation point in the wake of the disk is not

surprising, but its location is perhaps unexpected. Although the bulk concentration of surfactant should be maximized in the fluid adjacent to the coated regions of the disk, a finite adsorption time, t_{ads}, is required for the surfactant to adsorb to and then populate the air-water interface [32]. During the adsorption time, the disk has moved a distance $L=U_{disk}\ t_{ads}$, which, given the velocity of the disk and typically adsorption times for surfactant, can mean the minimum interfacial tension can exist a millimeter or more downstream of the disk. Although this argument can begin to explain the movement of the stagnation point into the wake of the disk, it still underpredicts the extent of movement. To fully understand the location of the stagnation point likely would require an understanding of how the three-dimensional (3D) flow around the disk affects the surfactant concentration near the interface.

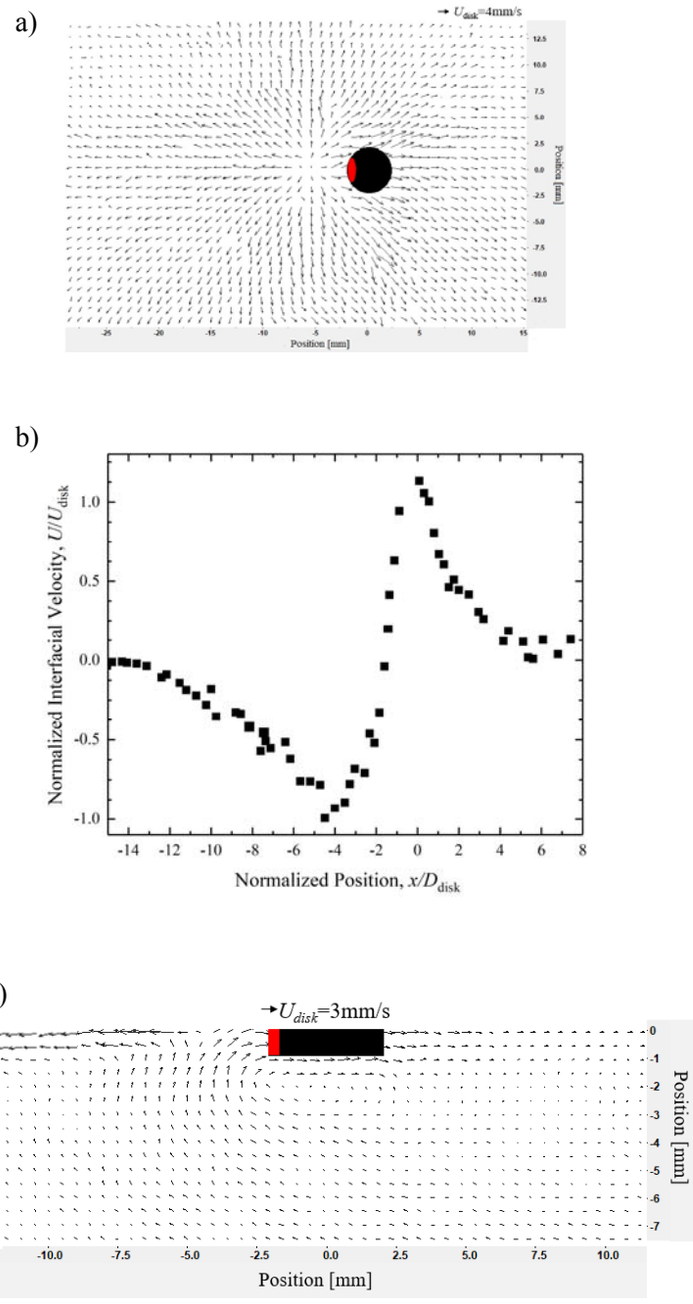

Figure 4. a) Plot of the Particle Image Velocimetry measurements of the flow field around a floating disk propelled by soap released from the disk in the area denoted by red region at its rear. b) Plot of the normalized interfacial centerline flow velocity, U/U_{disk}, as a function of normalized position, x/D_{disk} and c) a steady state disk velocity of U_{disk}=3mm/s. The center of the disk is placed at x=0. Scale bars are presented in each sub figure.

In order to better understand the interfacial flow, a centerline velocity profile of the interfacial flow upstream and downstream of the disk is shown in Figure 4b. Here, the interfacial velocity has been normalized by the disk velocity, U/U_{disk}, and the x-position has been normalized by the diameter of the disk, x/D_{disk}. The presence of the stagnation point can be seen more clearly here at a position of $x/D_{disk} = -1.5$. Note that $x/D_{disk} = 0$ represents the center of the disk. From the interfacial velocity profile, it can also be observed that the interfacial velocity in the wake decays at a slower rate compared to the velocity upstream of the disk. The far-field interfacial velocity was found to require a distance of $10D_{disk}$ to decay from its maximum to zero in the wake of the cylinder and a distance of $7D_{disk}$ to decay to zero upstream of the disk. For both the upstream and downstream of the disk, the interfacial velocity was found to decay like $1/x$ which is consistent with the predictions and experiments performed on interfaces dilated by a drop of surfactant in the absence of a Marangoni surfer [33]. The maximum velocity observed in the wake was roughly the same as the velocity of the disk $U/U_{disk}=-1$, while the maximum velocity upstream of the disk was roughly 10% higher, $U/U_{disk}=1.1$. This is expected as some relative velocity between the interface and the disk is needed to provide enough propulsive force to overcome the resistive drag force exerted by the water beneath the disk. In this steady-state, constant velocity regime, these forces are well balanced.

In order to better understand the details of the 3D flow profile around the disk, the laser light sheet was oriented vertically and passed into the Petri dish from below. The resulting PIV vector fields show the velocity profiles in a plane that bisects the disk along the direction of motion. A high speed camera capturing 100fps was used to image the flow from the side. In Figure 4c, the flow underneath the disk is presented after the disk has attained a steady state velocity of $U_{disk}=3$mm/s. The presence of an attached vortex rotating in the clockwise direction directly beneath the disk was observed. This vortex was found to be stable with time and remains attached for all other steady-state measurements made. This vortex exists in order to maintain conservation of mass in the Petri dish, if the interface is moving to the right then an equal mass of fluid below the interface must be moving back to the left.

3.3 Motion of Disk-Shaped Interfacial Swimmers Propelled by Isopropyl Alcohol

In this section, the effect of changing the strength of the propulsion agent is investigated by switching to isopropyl alcohol (IPA). The interfacial tension of IPA and the air-water interface saturated with surfactant are similar. However, IPA is a smaller, more mobile molecule that does not need to adsorb to the air-water interface to change the local interfacial tension. It simply needs to dissolve in the water and mix. The result is a fast-acting intense propulsion that is depleted much more quickly than the soap. The velocity profiles for a series of disks propelled by IPA are presented in Figure 5. The propulsive strength of the IPA was varied by diluting it from 100% to 20% by weight IPA with water to investigate the effect of varying propulsion strength. As the concentration of IPA was varied from 100wt% to 20wt% the surface tension of the IPA-water solution changed from σ = 22mN/m to 30mN/m. For the case of 20wt% IPA in water, a straight-line motion was observed similar to the case of soap propulsion with a maximum velocity of U_{disk}=25mm/s. The disk velocity decayed to zero quite quickly after a time period of t=2s. Unlike the case for soap discussed previously, steady-state motion was not observed for the case of 20wt% IPA or any of the other, higher concentrations. This is very different from the soap case. In fact, the average release rate of the IPA from the disk can be calculated to be approximately 0.5mg/s which is more than 10x faster than the case of soap. The acceleration and maximum velocity achieved appears to be directly related to the average release rate of the propulsion agent from the disk. Because the IPA is dissolved and depleted so quickly, to achieve extended propulsion, a reservoir of IPA rather than the thin coating used here is likely needed. Alternative approaches like viscosifying the IPA solution to be as viscous as the soap solution would reduce its release rate, but also reduce the strength of propulsion.

As the strength of IPA was increased from 30wt% to 50wt% to 100wt%, an increase in the maximum velocity of the disk was observed. From U_{disk}=60mm/s to U_{disk}=90mm/s and finally to U_{disk}=160mm/s respectively. With increasing propulsion strength came a new mode in the disk motion. As the concentration of IPA was increased to 30wt%, an initial straight-line translational motion was found to give way to a rotational motion of the disk. As discussed in the introduction, rotational motion of

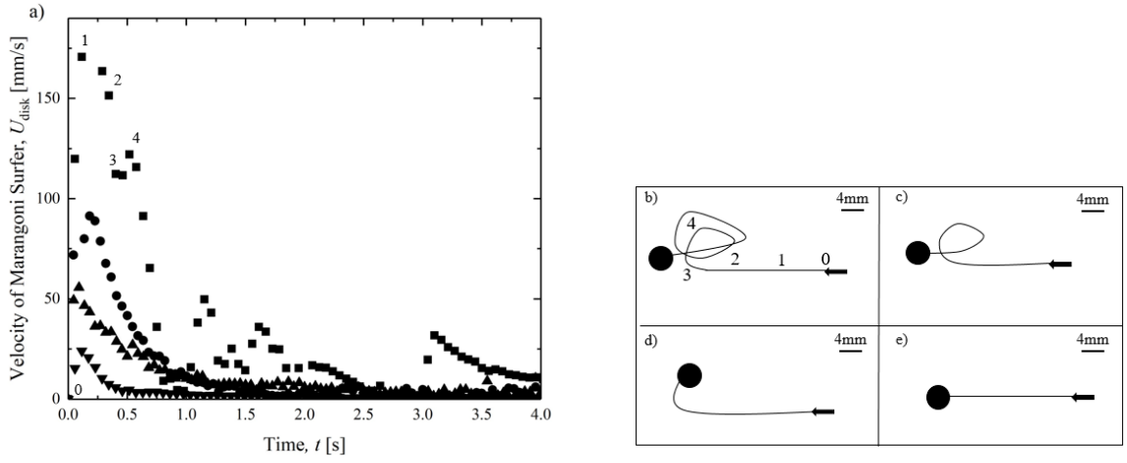

Figure 5. a) Plot of velocity of the cylindrical disk, U_{disk}, with time, t, for IPA strength of (▼) c=20wt%, (▲) 30wt%, (●) 50wt%, and (■) 100wt%. The path profile of the disk propelled by IPA showing the transition from a rotational motion to a straight-line translational motion for b) 100wt%, c) 50wt%, d) 30wt% and e) 20wt%.

Marangoni surfers has been seen before [11-14]. However, in each of these cases the rotation was induced by geometric asymmetries in the boat/surfer design. On further increasing the concentration of IPA to 50wt% and then to 100wt%, the number of the rotations and the angular velocity of the disk were found to increase as seen in the trajectories presented in Figure 5b-e. The increased number of rotations with increasing IPA concentration observed in Figure 5 is likely due to the increase in the duration of disk propulsion. The duration of disk motion was found to double as the IPA was increased from 20wt% to 100wt%. In all cases, rotation was only observed during the deceleration of the disk after the maximum velocity was achieved. Numbers have been added along the path of the 100wt% IPA cases in Figure 5b and the corresponding velocity data in 5a. This numbering shows a distinct correlation between the local peaks observed in the velocity data in Figure 5a and the onset of rotation of the disks in Figure 5b. We will show with PIV data in the next section that the local peak in velocity profile is due to the change in the drag coefficient on the disk resulting from the shedding of an attached vortex. It is this vortex shedding, and the resulting unbalanced torque on the disk, that causes the rotational motion of the disk.

It appears that there is a critical velocity that governs the transition between linear translation and rotation. The maximum velocities of the disk observed in the case of soap which did not rotate and 20wt% IPA solutions were found to be U_{disk}=15±2mm/s and U_{disk}=28±3mm/s respectively. While for the case of 30wt% IPA that did rotate the maximum velocity was found to be U_{disk}=65±5mm/s. The observed rotational motion of the disk can be more easily understood if the velocity is recast as a Reynolds number, $Re = \rho U_{disk} D_{disk} / \mu$. In Table 1, the maximum velocity and maximum Reynolds number along with the velocity and Reynolds number at the moment the disk was observed to rotate are presented for the different concentrations of IPA and soap. The data in Table 1, suggest that a critical Reynolds number governs the transition from a straight-line translational motion to a rotational motion. For the case of 20wt% IPA, which did not rotate, the maximum Reynolds number obtained was found to be *Re*=112±8. For the 25wt% case, the disk reached a maximum Reynolds number of *Re*=180±20 and began to spin after decelerating to a Reynolds number of *Re*=120±20. For the 100wt% IPA case, the maximum Reynolds number achieved was *Re*=640±30 and the spinning occurred at *Re*=450±40. The critical Reynolds number for transition is difficult to precisely determine due to the transient nature of the disk motion, but it is clear the maximum Reynolds number must be greater than that achieved for the 20wt% case and less than the 25wt% case. As a result, these experiments suggest that the critical Reynolds number required for the disk to spin is between $112 < Re_{critical} < 180$. To further investigate the interfacial flows around the disk, PIV measurements of the interfacial flow and the flow beneath the disk were performed.

IPA Concentration [wt%]	**Maximum Velocity** U_{max} [mm/s]	**Maximum Reynolds Number** Re_{max}	**Velocity Prior to Rotation** $U_{rotation}$ [mm/s]	**Reynolds Number Prior to Rotation** $Re_{rotation}$
100%	160 ± 8	640 ± 30	120 ± 10	450 ± 40
50%	100 ± 10	400 ± 40	65 ± 10	280 ± 40
30%	65 ± 5	260 ± 20	40 ± 5	160 ± 20
25%	45 ± 5	180 ± 20	30 ± 5	120 ± 20
20%	28 ± 2	112 ± 8	NA	NA

Soap	15 ± 3	60 ± 10	NA	NA

Table 1. Variation of the velocity and Reynolds number for different concentration of IPA and soap used to propel the disk.

3.4 PIV of a Disk-Shaped Interfacial Swimmer Propelled by IPA

In this section, the PIV measurements of the flow field in the water around a disk-shaped Marangoni swimmer propelled by IPA are presented. Interfacial PIV measurements for the case of a stationary disk, U_{disk}=0mm/s, is presented below in Figure 6. Like the case of soap, a radially outward flow was observed downstream of the disk on the side where the alcohol was applied. Unlike in the case of soap, the presence of a pair of vortex can be observed upstream of the disk in Figure 6a. The vortices became more and more distinct as time progressed. Although the vortices of the stationary disk were observed to grow in intensity with time as seen in Figure 6b, they did not shed. The origin of these vortices arose from a feature in the IPA-induced Marangoni flow that was not intuitively expected. Upstream of the disk, the interfacial flow is not radially outward instead, the flow upstream of the disk is directed towards the disk, where it then flows around and beneath the disk and into the wake downstream of the disk. This can be seen more clearly in Figure 6c-d, which shows the PIV vector fields from beneath the stationary disk. The observed flow reversal is likely due to the need for mass conservation to replace the interfacial fluid that is quickly dialating outward from the region of low surface tension in the wake of the disk. It is clear that the presence of the disk has a large impact on the resulting Marangoni flow field. For instance, if one deposits a drop of alcohol on the water surface without a disk present, a purely radial flow is observed on the interface. The main difference between the soap and the alcohol case is from the strength of the flow. Here, the outward velocity of the interface was found to reach more than 150 ± 10m/s while in the case of soap only 50 ± 10mm/s was reached. The difference is enough to change the character of the flow and the dynamics of the disk motion once it is released. In Figure 6c-d, the Marangoni flow field underneath the stationary disk induced by 100wt% IPA is presented. A vortex is clearly visible downstream of the disk. With time, this vortex was observed to shed and move downstream away from the stationary disk. At t=1s the center of the vortex was found to be at x=-12mm and was found to move to x=-16mm at t=2s. The magnitude of

the strength of vortex was found to decrease from ω=15s^{-1} at t=1s to ω=5s^{-1} at t=2s as the vortex was found to diffuse into the bulk as it moved away from the disk. Compared to the case of soap, for which the vortices were found to be shallow and to rotate in close proximity to the interface, the vortices observed in

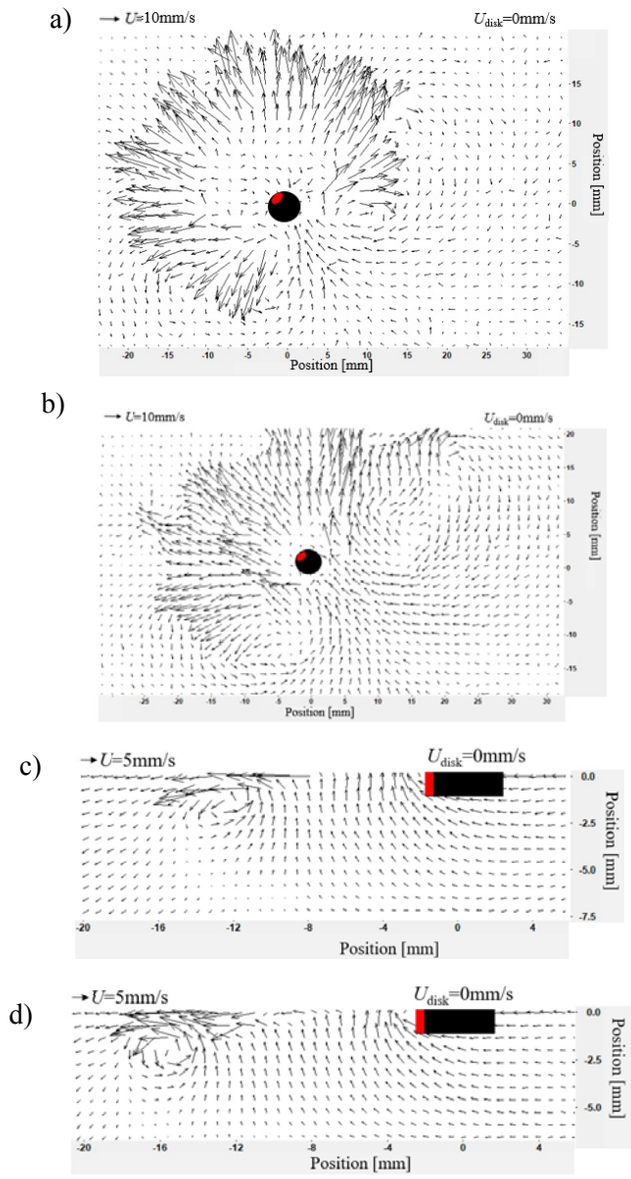

Figure 6. Plot of the Particle Image Velocimetry measurements of the flow field upstream and downstream of a stationary disk (U_{disk}=0mm/s) within a Marangoni flow field induced by the release of 100% IPA from the back of the disk in the area denoted in red. a)-c) and b)-d) denote time instances t=1s and t=2s after disk immersion, respectively.

the case of IPA were found to be much deeper and extending further from the surface into the bulk. The strength of the vortices was also found to be larger for the case of IPA.

In Figure 7a-b, the Marangoni flow along the interface and vorticity maps around a disk during its transient motion is shown at different times following deposition onto the interface. Here we are presenting the case of 30wt% IPA. The resulting flow field is quite different from the case of a stationary disk. A radially outward flow originating from the wake of the disk was observed to propel the disk in the direction away from where IPA was introduced into the water and the surface tension was reduced. The attached interfacial vortices that were observed for the case of a stationary disk in Figure 6a-b were observed to shed as the disk was propelled forward. As the disk moved across the interface, two counter-rotating vortices attached were observed to form and remain attached to the side of the disk along its equator. These vortices were not initially obvious, t<0.3s, likely because of the resolution limitations of our PIV, but appeared quite visibly at longer times, t>0.3s, as the disk moved away from the start-up vortices that were formed upon deposition and shed in the wake of the disk. Interestingly, with the disk free to surf across the interface, the reversed flow observed for the stationary disk in Figure 6, was not seen, but instead replaced by a strong propulsive flow easily observed upstream of the disk where the interfacial tension is the largest. The formation and shedding of these interfacial vortices is not observed for the case of soap for which the maximum Reynolds number achieved was just Re=60±10. For the IPA cases, the Reynolds number was much greater, Re>200. The presence of interfacial vortices is thus clearly an inertial effect.

PIV measurements was also performed to investigate the flow underneath the disks propelled by IPA. In Figure 7c, the flow field induced by 30% IPA underneath the interface is presented for a disk t=0.5s after its release. The initial vortex produced at start-up as the disk was immersed and released onto the interface was observed to shed after 0.1s. That start-up vortex can still be seen in Figure 7c, rotating counter-clockwise with positive vorticity at the time far left of the image centered around x=-15mm. After the initial start-up vortex was shed a second vortex attached to the bottom of the disk was observed to grow and to rotate in the opposite direction, clockwise with negative vorticity. Compared to the vortex observed in the case of soap, the attached vortex was not found to form beneath the center of the disk, but offset

downstream towards the wake. This attached vortex was found to shed as the disc rotated. This is also quite different from the case of the soap for which the attached vortex was not observed to shed.

During the start-up flow, three to four lobes of vortices were observed at the point of release for all the cases of different concentrations of IPA. For the case of 20wt% IPA, a straight-line motion similar to that of soap was observed. In this case, after the start-up vortices were shed, the subsequent vortices attached to the side and bottom of the disk shown in Figure 8a did not shed. As the strength of IPA in

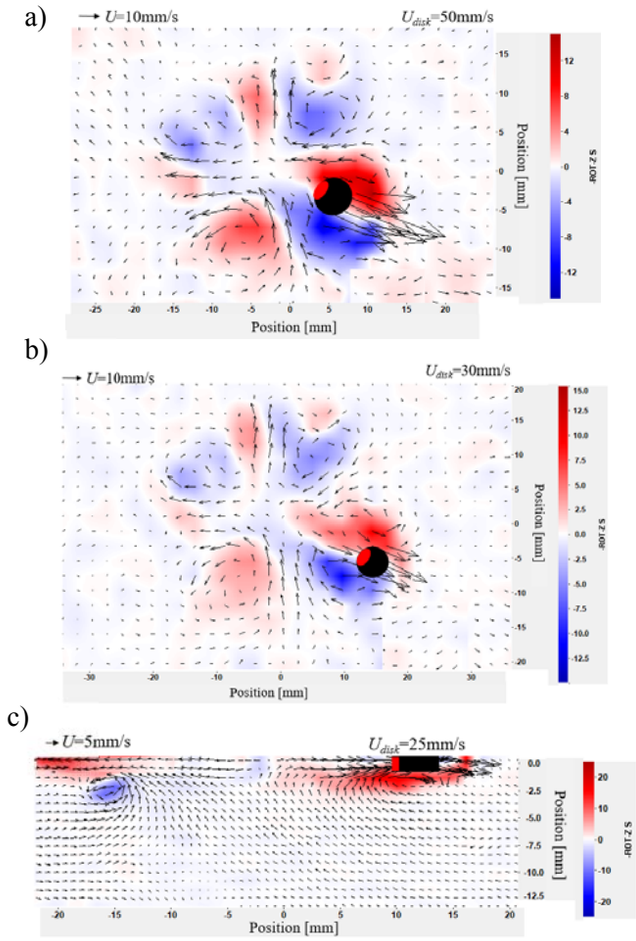

Figure 7. Plot of the Particle Image Velocimetry measurements of the flow field upstream and downstream of a disk propelled by IPA (30wt%) released on the back of the disk in the area denoted in red moving along its initial trajectory at a time of a) t=0.2 after release and a disk velocity of U_{disk}=50mm/s, b) t=0.3s and U_{disk}=40mm/s and c) flow field underneath the moving disk with disk velocity of U_{disk}=25mm/s at t=0.5s. The center of the disk was released at (0,0). The scale bar on the right shows the magnitude of the strength of vorticity.

Figure 8b was increased to 30wt%, the pair of counter-rotating vortices remained attached to the side of the disk for roughly 20mm as the disc moved along its initial line of motion. However, with time, the vortex to the port side of the disk was observed to shed, resulting in a rotational motion of the disk. As the disk rotated away from its original trajectory, a jet of fluid was observed to move past its port side moving the disk to its starboard side. Multiple experiments were performed for each IPA concentration. From those experiments, it was found that the side from which the vortex was shed was random and not biased to one side of the disk or the other. Similar vortex instability was observed for the case of 50wt% and 100wt%, although, with increasing IPA concentration, the shedding of vortex occurred at a higher disk velocity and Reynolds number. In each case, the shedding of vortex coincided with the transition from a straight-line

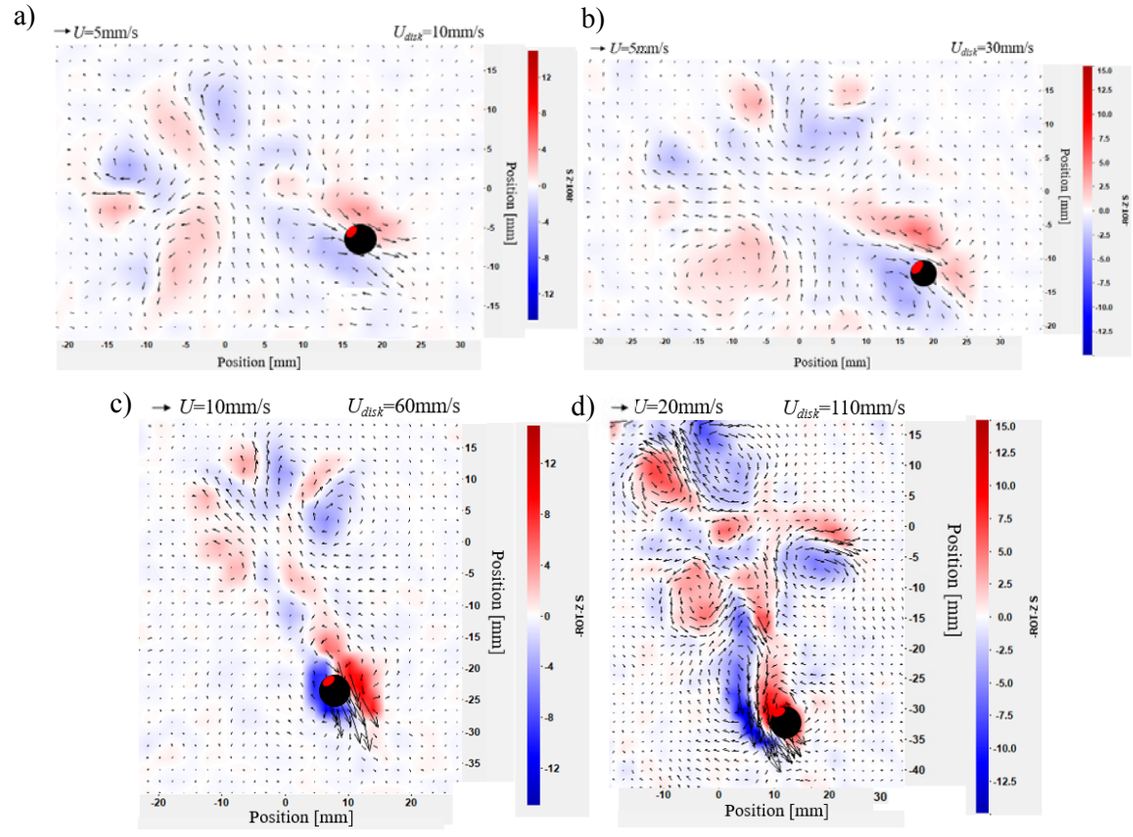

Figure 8. Plot of the Particle Image Velocimetry measurements of the flow field upstream and downstream of a disk propelled by IPA released on the back of the disk in the area denoted in red. The strength of the propulsion was varied by changing the IPA concentration from a) 20wt%, to b) 30t%, to c) 50wt%, and finally to d) 100wt%. The initial point of release in each case was at (0,0). The scale bar on the right shows the magnitude of the strength of vorticity

motion to a rotational motion. The shedding vortex results in both a time-dependent drag and lift coefficient on the disk resulting in an unbalanced torque that rotates the disk away from its straight-line trajectory and into an orbital path that continues until the IPA was depleted. As described previously, the strength of the rotational motion was found to increase with increasing IPA concentrations and is directly related to the vorticity of the shed vortex and the subsequent strength of the resulting jet of fluid.

3.5 Effect of Interface Curvature on the Motion of a Disk-Shaped Interfacial Swimmer

In the previous sections, the air-water interface was kept flat and the Petri dish was large enough to avoid interactions between the disk and the wall of the container. Here we purposefully introduce end-effects and interfacial curvature to investigate their impact on the motion of a disk-shaped interfacial swimmer. In this section, IPA was used as the propulsion agent. The experiments were performed in a Petri dish of diameter D=86mm and the cylindrical disk of diameter D_{disk}=4mm was released with the help of tweezers. As described in the experimental section, the interfacial curvature was set by pinning the air-water interface on the sharp edge of the Petri dish and then either adding or subtracting water to obtain the desired curvature. The effect of interfacial curvature at the boundary was investigated using 100% IPA as the propulsion agent. As seen in Figure 9, an initial straight-line motion was observed in all cases. For the flat interface, the disk was observed to rotate and go through a series of loops before reaching the boundary wall. This type of motion was observed for concentrations down to 25wt% IPA. However, for the case of 20wt% IPA, which had a lower disk velocity and a lower Reynolds number, the disk was observed to have directly impacted the wall without rotation. As the disk approached the wall, it must move through an adverse pressure gradient as the interfacial and bulk fluid velocity must come to rest at the wall. As a result, a pressure field is produced that decelerates the disk. If the disk does not approach the wall along a perfectly radial path and is at a high enough velocity, this pressure field can provide a torque that can rotate the disk before it impacts the wall and can cause the attached vortices to shed as was observed for all the cases above 25wt% IPA. As before, both clockwise and counter-clockwise motions were observed based on the initial

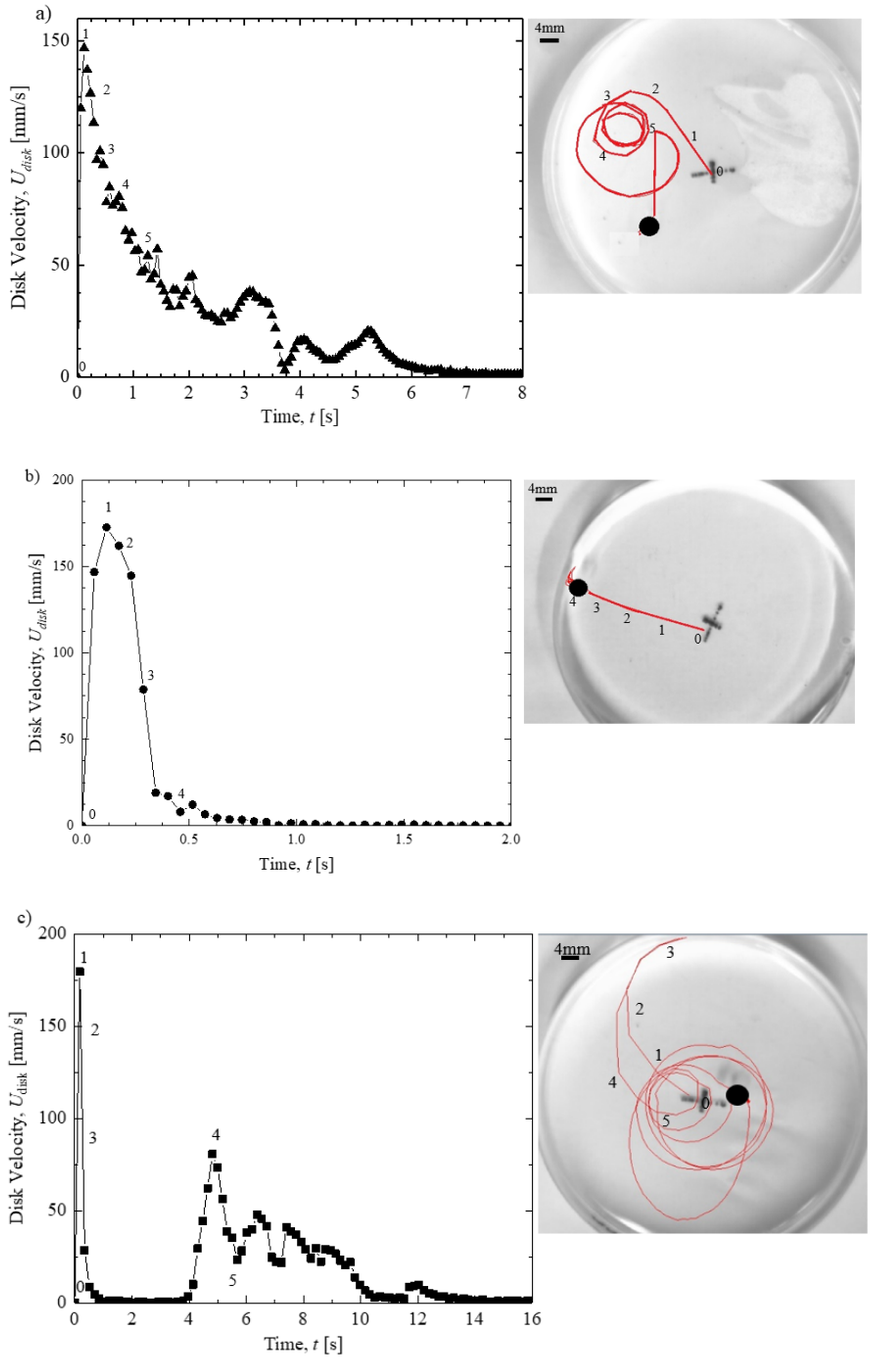

Figure 9. Plot of the disk velocity magnitude, U_{disk}, as a function of time, t, for a disk propelled along an air-water interface using IPA. Results are shown for a) a flat, b) a convex, and c) a concave interface at the boundary of the Petri dish. The images on the right show a trace of the trajectory of the disk. The numbers on the images on the right shows the position of the disk at different times and its corresponding velocity can be found out from the velocity profile on the left.

100wt% IPA data in Figure 9a, which indicate times at which rotational motion of the disk was initiated. The average radius of curvature of the loops and the average period of rotation were found to be R=6±2mm and T=0.4±0.1s, respectively for the case of flat interface. A maximum velocity of between U_{disk}=150m/s and 180m/s was observed in all the cases of 100% IPA. One important point to note here is that, for the unconfined disk, a critical maximum Reynolds number of Re=120±20 was needed to observe disk rotation whereas, for the case of a confined disk moving along a flat interface, a significantly lower critical Reynolds number of Re=50±10 was needed to observe disk rotation as it approached the confining wall.

For the case of a convex interface at the boundary of the Petri dish, as shown in Figure 9b, the disk propelled by 100wt% IPA followed a straight-line motion towards the wall and came to rest along the boundary. A similar result was observed for all the IPA concentrations tested. In all cases, the disk never resumed motion even though interfacial motion could still be observed around the arrested disk. Unlike in the case of the flat interface, an increase in the velocity of the disk was observed as it approached to within a diameter of the wall. This acceleration is likely due to the gravitational acceleration of the disk down the convex interface which is likely the reason why convex interfacial curvature at a boundary appears to eliminate disk rotation.

In the case of a concave interface curvature at the boundary of the Petri dish, as shown in Figure 9c, the disk propelled by 100wt% IPA was found to follow a straight-line motion towards the wall, hit the wall, and remained pinned to the wall for 4s before propelling itself away from the wall. As the disk moved away from the boundary, a rotational motion similar to the flat interface case was observed. In some cases, the disk rotation observed for the concave interface was centered near the center of the Petri dish while in other cases the rotation was observed along the boundary of the Petri dish like in Figure 9a. Interestingly, for the case of the flat interface, the rotation was always observed as it approached the boundary wall. As in the case of the flat surface, no rotation was observed for IPA concentrations below 25wt%. The average radius of curvature of the rotational motion and the average period of rotation for the concave case were found to be R=10±2mm and T=2.0±0.4s respectively resulting in a rotational velocity of

$U_{rotational} = 2\pi R / T = 42 \pm 5\text{mm/s}$. The rotational velocity is significantly smaller than the value of $U_{rotational} = 110 \pm 10\text{mm/s}$ observed for the flat interface which shows that interfacial curvature can have quite a large impact on the dynamics of a self-propelled swimmer.

4. Conclusion

In the experiments presented in this paper, we have investigated the dynamics of a disk-shaped Marangoni swimmer propelled by either soap or isopropyl alcohol (IPA) applied to the back of the disk. Both IPA and soap reduce the surface tension of water. The resulting surface tension gradient propels small objects, like the disks studied here, across the interface and produces a Marangoni flow. The motion of the thin disk was tracked over time and the interfacial and bulk flows were characterized using Particle Image Velocimetry (PIV). Upon insertion of the disk onto the interface, the surface tension gradient caused the interface to dilate, spreading out radially from the side of the disk where the propulsion agent was applied and driving the motion of the floating disks. The interfacial fluid velocities and the resulting disk velocities were significantly larger when IPA was used as the propulsion agent. The maximum Reynolds number of $Re = 60$ was achieved by the disk in the case of soap, whereas, a Reynolds number greater than $Re > 600$ was achieved for IPA. At these intermediate Reynolds numbers, the role of inertia can no longer be ignored. Beyond a Reynolds number of $Re > 100$, the interfacial flow around the disk was found to separate and a pair of counter-rotating interfacial vortices were observed on the sides of the disk. At even larger Reynolds numbers, $Re \geq 180$, these vortices became unstable and were eventually shed. The unbalanced torques resulting from vortex shedding destabilized the straight-line translational motion of the disk-shaped Marangoni surfers and forced the disks to spin. This critical Reynolds number may limit the size of self-propelled object, or speed at which they can use linear motion in the bottom-up fabrication of small functional systems [34].

Although a number of studies have used asymmetries in the design of Marangoni surfers to induce spontaneous interfacial spinning [11, 12], this study is the first to demonstrate that a geometrically

axisymmetric Marangoni surfer can also rotate. The transition from translational to rotational motion is a strongly dependent on Reynolds number. As a result, similar rotational motion is not expected for small Marangoni surfers like bacteria because the Reynolds number of their motion is well below the critical Reynolds number observed here. However, the interfacial motion of water-walking insects falls quite nicely into this intermediate Reynolds number flow regime. Take for example, the whirligig beetles which are known to propel themselves by releasing a surface active substance into the water [35]. Velocities as high as 64cm/s have been observed for the case of whirligig beetles which translates into Reynolds number of over $Re > 1000$. Observations of whirligig beetle motion shows that they often spin giving rise to their name [35]. The high interfacial swimming velocities might give these beetles an advantage in predator avoidance, while the rotational motion induced by vortex shedding may help in evading predators by rapidly and perhaps unpredictably changing the trajectory of the beetle once it has propelled itself beyond the critical Reynolds number.

Changing the propulsion agent was found to result in a number of additional effects beyond just changing the maximum velocity achieved by the disk. The soap was found to slowly dissolve from the disk over the course of minutes, while the IPA dissolved in seconds. The result was a strong impulsive propulsion from the IPA resulting in a fast acceleration followed by a slow deceleration of the disk. For the IPA, steady state translational velocity was never achieved even in the case where rotational motion was not observed. However, when soap was used as the propulsion agent, a slower acceleration was observed and a steady state velocity was achieved and maintained for quite some time. By achieving a steady-state velocity, disks propelled by soap appeared to a system that is more appropriate for fundamental studies where the effects of transient motion are undesirable. Although only the IPA cases displayed interfacial vortices attached to the side of the disk, both soap and IPA showed the presence of an attached vortex right beneath the disk and the presence of a stagnation point along the interface in its wake. This stagnation point represents the location of the lowest surface tension along the interface and the point from

which the surface radially dilates. The location of the stagnation point was found to move further into the wake with increasing disk velocity.

By allowing the disk-shaped Marangoni surfers to interact with the edge of the Petri dish, the effects of the boundary and interface curvature were investigated. The presence of wall leads to an adverse pressure gradient which brought the interfacial flow to rest and decelerated the disks as they approached. For the flat interface, the presence of the boundary caused the disks to spin and rotate away from the wall. The critical Reynolds number for rotation near the wall was significantly less, $Re = 50\pm10$, than for an unbounded flow. The presence of concave or convex curvature at the edge of the Petri dish resulted in an additional repulsive or attractive force on the disk due to gravity, which modified the flat interface behavior making it more likely to spin from or pin to the wall, respectively. The interactions between the disks and the wall are a useful first step in understanding the interaction between multiple Marangoni surfers on an interface. While the interface around the disk-shaped Marangoni surfer used here was essentially flat, interfacial curvature effects can be extremely strong at these length scales. Quite a bit of research has already been done to investigate the use of interfacial curvature and surface tension to induce self-assembly of non-propelled objects into small scale structures [36]. Taking that work one step further, if one can understand how particles propelled by interfacial tension gradients aggregate at an interface, one might be able to better understand and control the dynamics of particle aggregation and assembly making it possible to build even more complex structures.

Acknowledgements

The authors would like to thank NSF for financial support of this research under grants CBET – 1705519 (J.P.R) and CBET-1749634 (H.M).

References

1. Scriven, L.E. and C.V. Sternling, *The Marangoni effects.* Nature, 1960. **187**: p. 186-188.
2. Angelini, T.E., et al., *Bacillus subtilis spreads by surfing on waves of surfactant.* PNAS, 2009. **106**: p. 18109-18113.
3. Fauvart, M., et al., *Surface tension gradient control of bacterial swarming in colonies of Pseudomonas aeruginosa.* Soft Matter, 2012. **8**: p. 70-76.
4. Schildknecht, H., *Chemical ecology-a chapter of modern natural products chemistry.* Angewandte Chemie International, 1976. **15**: p. 214-222.
5. Andersen, N.M., *A comparative study of locomotion on the water surface in semiaquatic bugs (Insects, Hemiptera, Gerromorpha).* Vidensk. Meddr. Dan. Naturhist. Foren. , 1976. **139**: p. 337-96.
6. Betz, O., *Performance and adaptive value of tarsal morphology in rove beetles of the genus Stenus (Coleoptera, Staphylinidae).* J. Exp. Biol., 2002. **205**: p. 1097-113.
7. Bush, J.W. and D.L. Hu, *Walking on water: biolocomotion at the interface.* Annu. Rev. Fluid Mech., 2006. **38**: p. 339-369.
8. Rayleigh, L., *Measurements of the amount of oil necessary in order to check the motions of camphor upon water.* Proc. R. Soc. Lond., 1889. **47**: p. 364-367.
9. Suematsu, N.J., et al., *Mode-switching of the self-motion of a camphor boat depending on the diffusion distance of camphor molecules.* The Journal of Physical Chemistry C, 2010. **114**(21): p. 9876-9882.
10. Renney, C., A. Brewer, and T.J. Mooibroek, *Easy demonstration of the Marangoni Effect by prolonged and directional motion:"Soap Boat 2.0".* Journal of Chemical Education, 2013. **90**(10): p. 1353-1357.
11. Nakata, S., et al., *Self-rotation of a camphor scraping on water: new insight into the old problem.* Langmuir, 1997. **13**(16): p. 4454-4458.
12. Koyano, Y., et al., *Relationship between the size of a camphor-driven rotor and its angular velocity.* Physical Review E, 2017. **96**(1): p. 012609.
13. Takabatake, F., et al., *Spontaneous mode-selection in the self-propelled motion of a solid/liquid composite driven by interfacial instability.* The Journal of chemical physics, 2011. **134**(11): p. 114704.
14. Nagai, K.H., et al., *Rotational motion of a droplet induced by interfacial tension.* Physical Review E, 2013. **87**(1): p. 013009.
15. Gidituri, H., M.V. Panchagnula, and A. Pototsky, *Dynamics of a fully wetted Marangoni surfer at the fluid–fluid interface.* Soft matter, 2019. **15**(10): p. 2284-2291.
16. Soh, S., K.J. Bishop, and B.A. Grzybowski, *Dynamic self-assembly in ensembles of camphor boats.* The Journal of Physical Chemistry B, 2008. **112**(35): p. 10848-10853.
17. Soh, S., M. Branicki, and B.A. Grzybowski, *Swarming in shallow waters.* The Journal of Physical Chemistry Letters, 2011. **2**(7): p. 770-774.
18. Lauga, E. and A.M. Davis, *Viscous marangoni propulsion.* Journal of Fluid Mechanics, 2012. **705**: p. 120-133.
19. Würger, A., *Thermally driven Marangoni surfers.* Journal of Fluid Mechanics, 2014. **752**: p. 589-601.
20. Masoud, H. and H.A. Stone, *A reciprocal theorem for Marangoni propulsion.* Journal of Fluid Mechanics, 2014. **741**.
21. Masoud, H. and M.J. Shelley, *Collective surfing of chemically active particles.* Physical review letters, 2014. **112**(12): p. 128304.
22. Vandadi, V., S.J. Kang, and H. Masoud, *Reverse Marangoni surfing.* Journal of Fluid Mechanics, 2017. **811**: p. 612-621.
23. Kralchevsky, P.A. and K. Nagayama, *Capillary interactions between particles bound to interfaces, liquid films and biomembranes.* Adv. Coll. Int. Sci., 2000. **85**: p. 145-192.

24. Vella, D. and L. Mahadevan, *The "Cheerios Effect".* American Journal of Physics, 2005. **73**: p. 817-825.
25. Zeng, C., H. Bissig, and A.D. Dinsmore, *Particles on droplets: from fundamental physics to novel materials.* Solid State Com., 2006. **139**: p. 547-556.
26. Daniello, R., et al., *The effect of contact angle and density on the orientation, stability and assembly of floating cubes.* Phys. Rev. E, 2014. **89**: p. 023014.
27. Kassuga, T.D. and J.P. Rothstein, *Buckling of particle laden interfaces.* J. Colloid Int. Sci., 2015. **448**: p. 287-296.
28. Kassuga, T.D. and J.P. Rothstein, *The Effect of Shear and Confinement on the Buckling of Particle-Laden Interfaces* J. Phys.: Condens. Matter, 2016. **28**(2): p. 025101.
29. Cavallaro, M., et al., *Curvature-driven capillary migration and assembly of rod-like particles.* Proc. Natl. Acad. Sci., 2011. **108**: p. 20923-20928.
30. Loudet, J.C. and B. Pouligny, *How do mosquito eggs self-assemble on the water surface?* Eur. Phys. J. E, 2011. **34**: p. 76.
31. Sane, A., S. Mandre, and I. Kim, *Surface tension of flowing soap films.* Journal of Fluid Mechanics, 2018. **841**.
32. Yunfei, H., et al., *Surfactant adsorption onto interfaces: measuring the surface excess in time.* Langmuir, 2012. **28**(6): p. 3146-3151.
33. Akella, V., et al., *Dynamics of a camphoric acid boat at the air–water interface.* Physics Letters A, 2018. **382**(17): p. 1176-1180.
34. Ismagilov, R.F., et al., *Autonomous Movement and Self-Assembly.* Angew. Chem. Int. Ed., 2002. **41**: p. 652-654.
35. Vulinec, K., *Swimming in whirligig beetles (Coleoptera: Gyrinidae): a possible role of the pygidial gland secretion.* The Coleopterists' Bulletin, 1987: p. 151-153.
36. Whitesides, G.M. and B. Grzybowski, *Self-assembly at all scales.* Science, 2002. **295**(5564): p. 2418-2421.

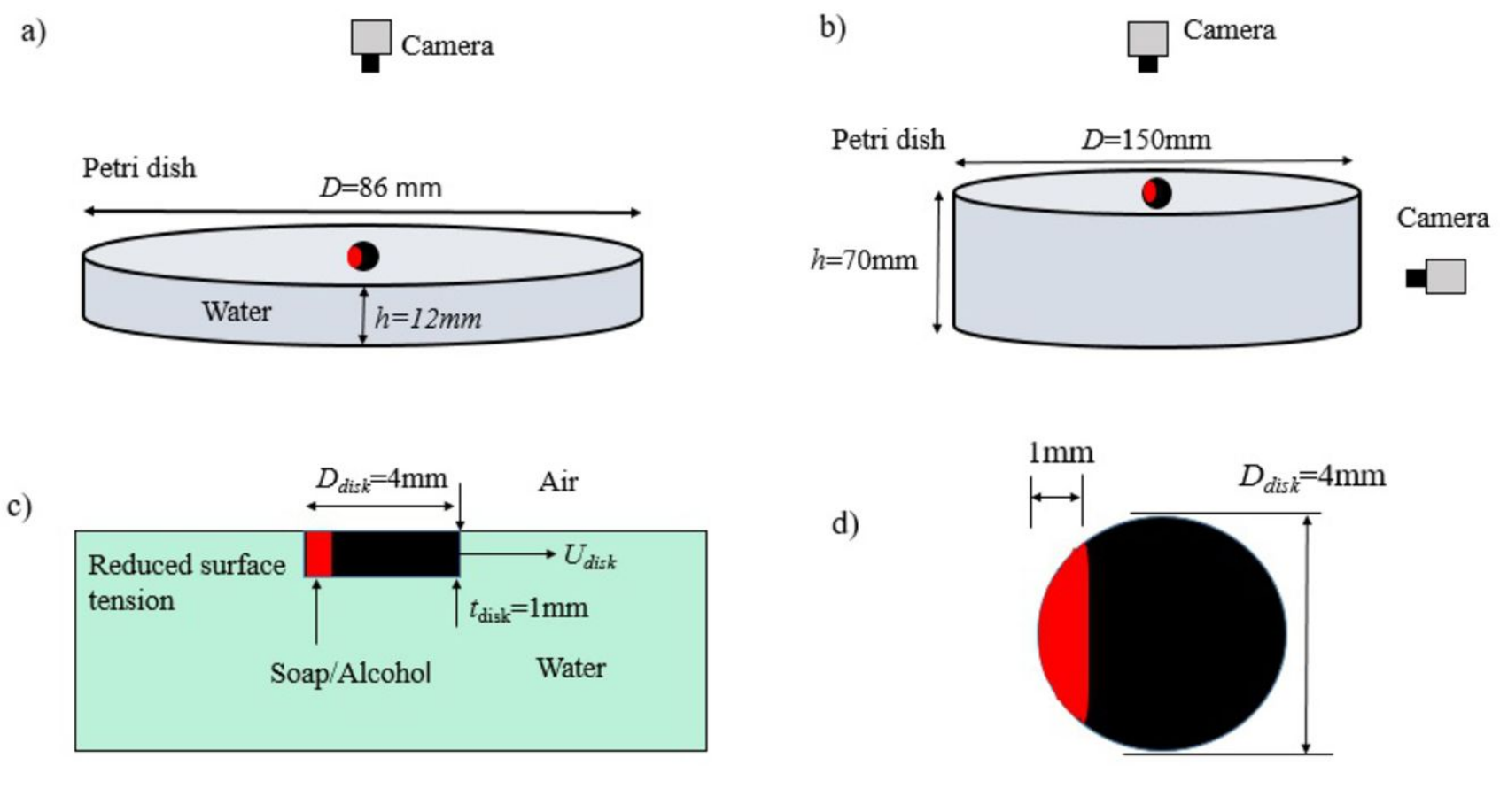
a)
Camera
Petri dish
D=86 mm
Water
h=12mm
b)
Camera
Petri dish
D=150mm
h=70mm
Camera
c)
D_disk=4mm
Air
Reduced surface tension
U_disk
t_disk=1mm
Soap/Alcohol
Water
d)
1mm
D_disk=4mm

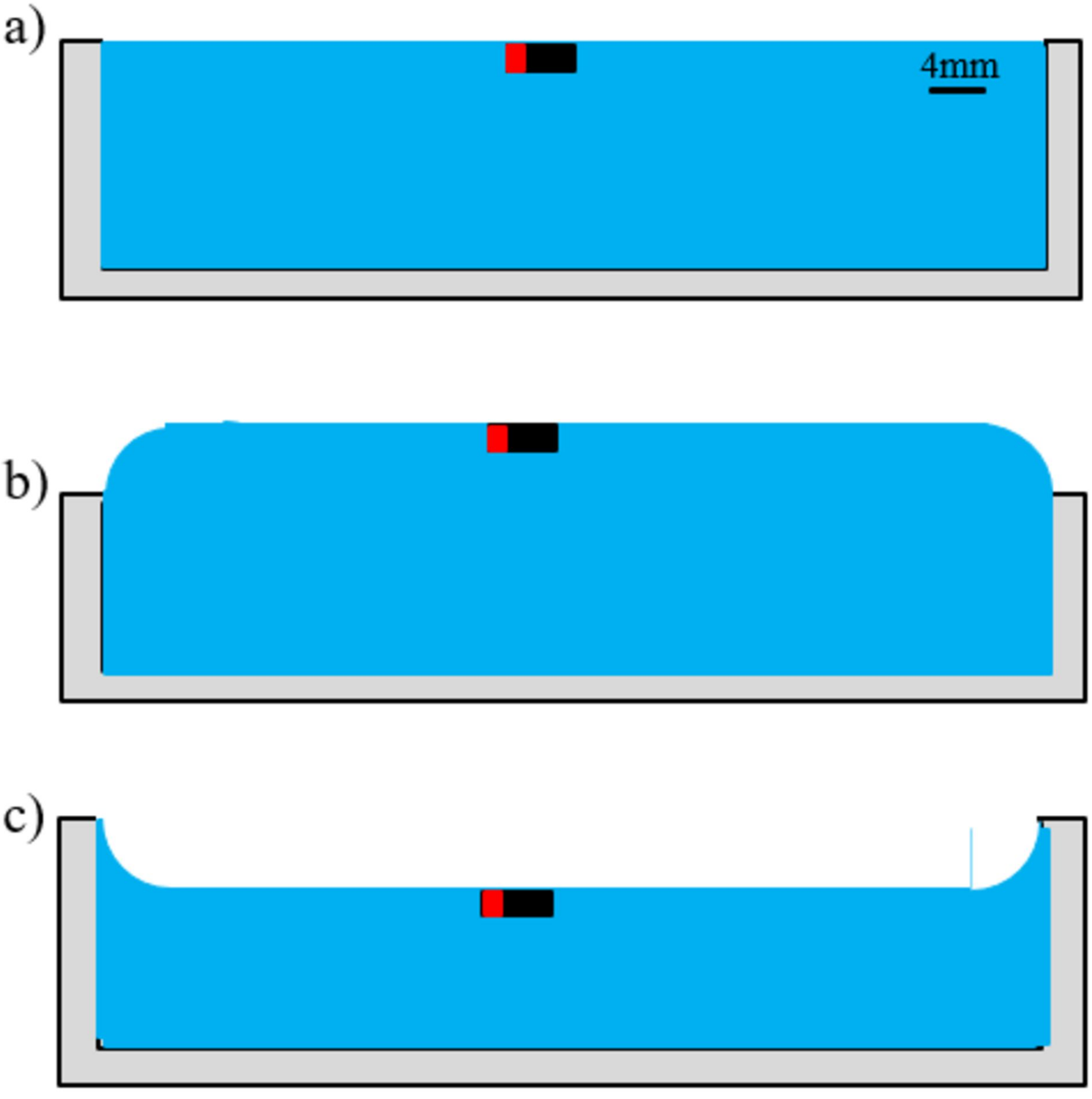
a)
4mm
b)
c)

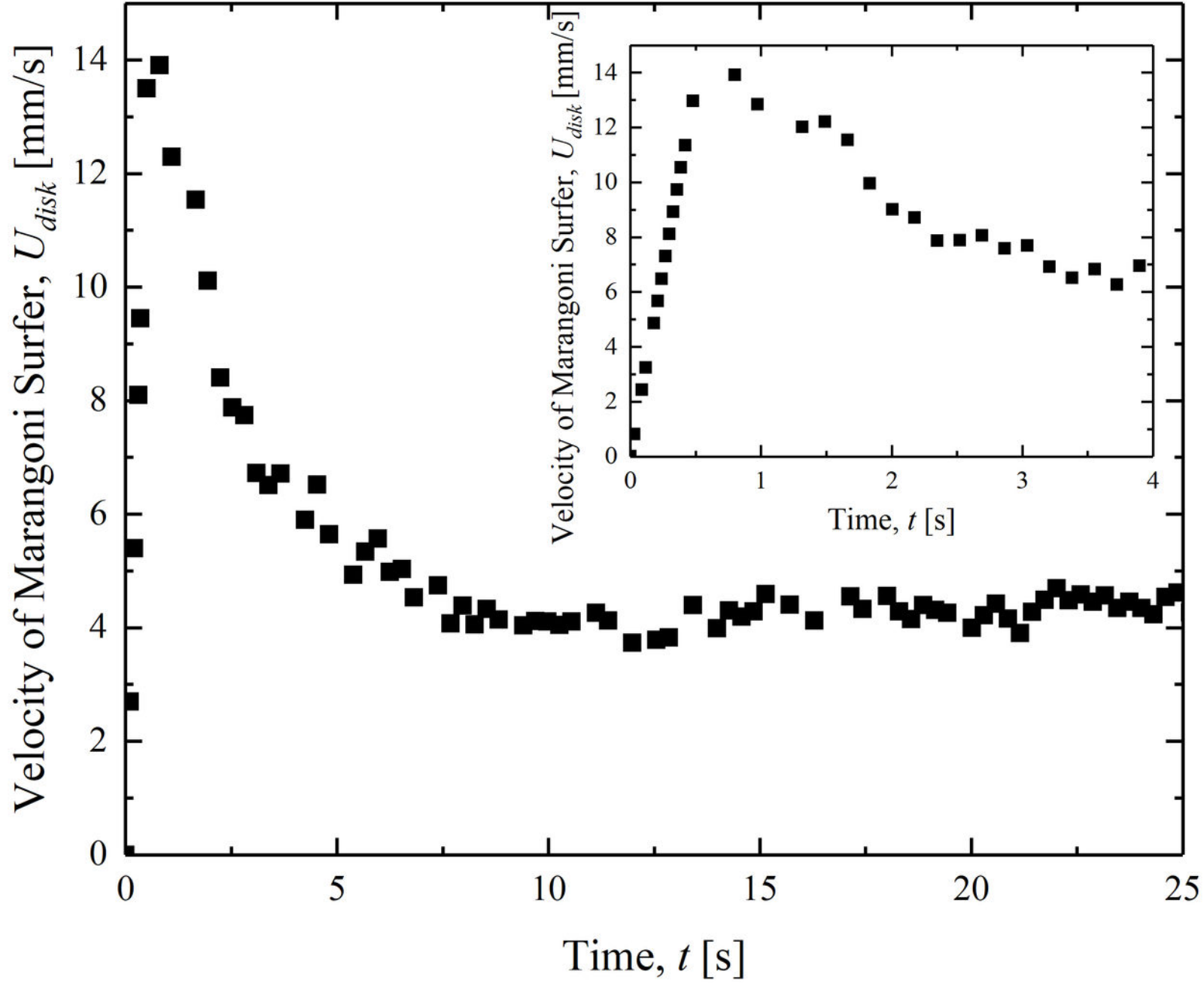
Velocity of Marangoni Surfer, U_{disk} [mm/s]
Time, t [s]
0
2
4
6
8
10
12
14
0
5
10
15
20
25
Velocity of Marangoni Surfer, U_{disk} [mm/s]
Time, t [s]
0
2
4
6
8
10
12
14
0
1
2
3
4

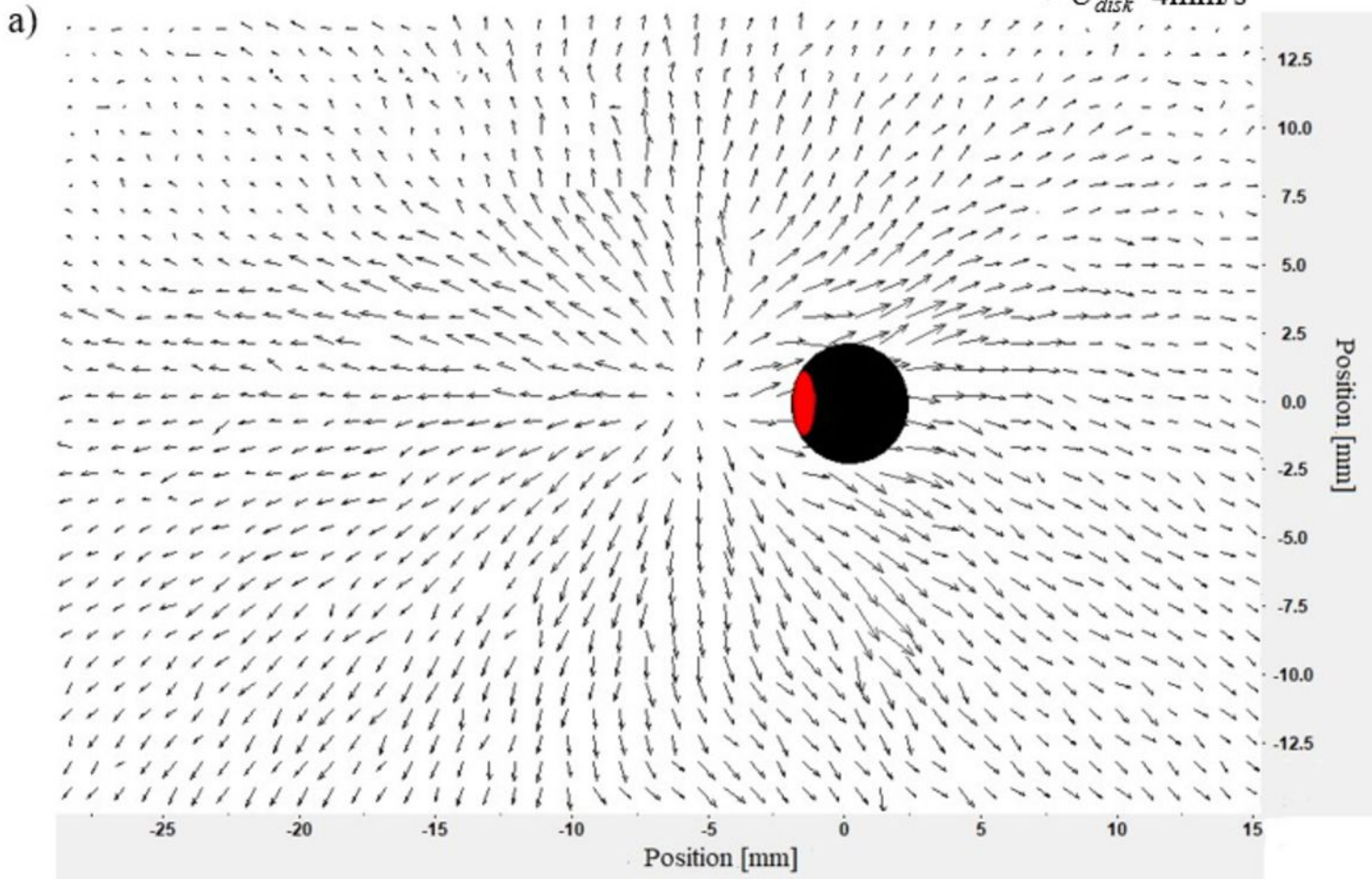
a)
→ U_{disk}=4mm/s
12.5
10.0
7.5
5.0
2.5
0.0
-2.5
-5.0
-7.5
-10.0
-12.5
Position [mm]
-25
-20
-15
-10
-5
0
5
10
15
Position [mm]

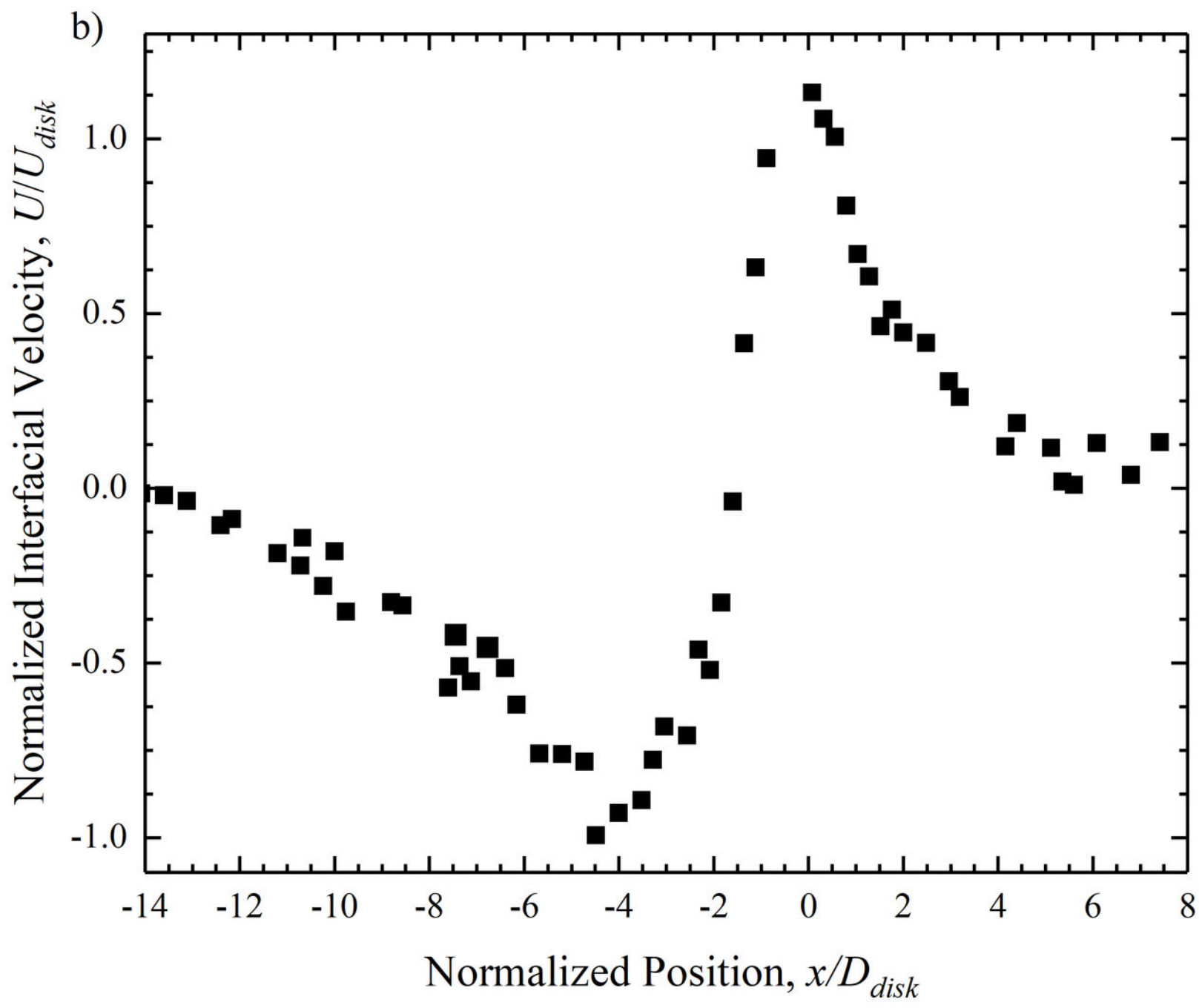
b)
Normalized Interfacial Velocity, U/U_{disk}
1.0
0.5
0.0
-0.5
-1.0
-14
-12
-10
-8
-6
-4
-2
0
2
4
6
8
Normalized Position, x/D_{disk}

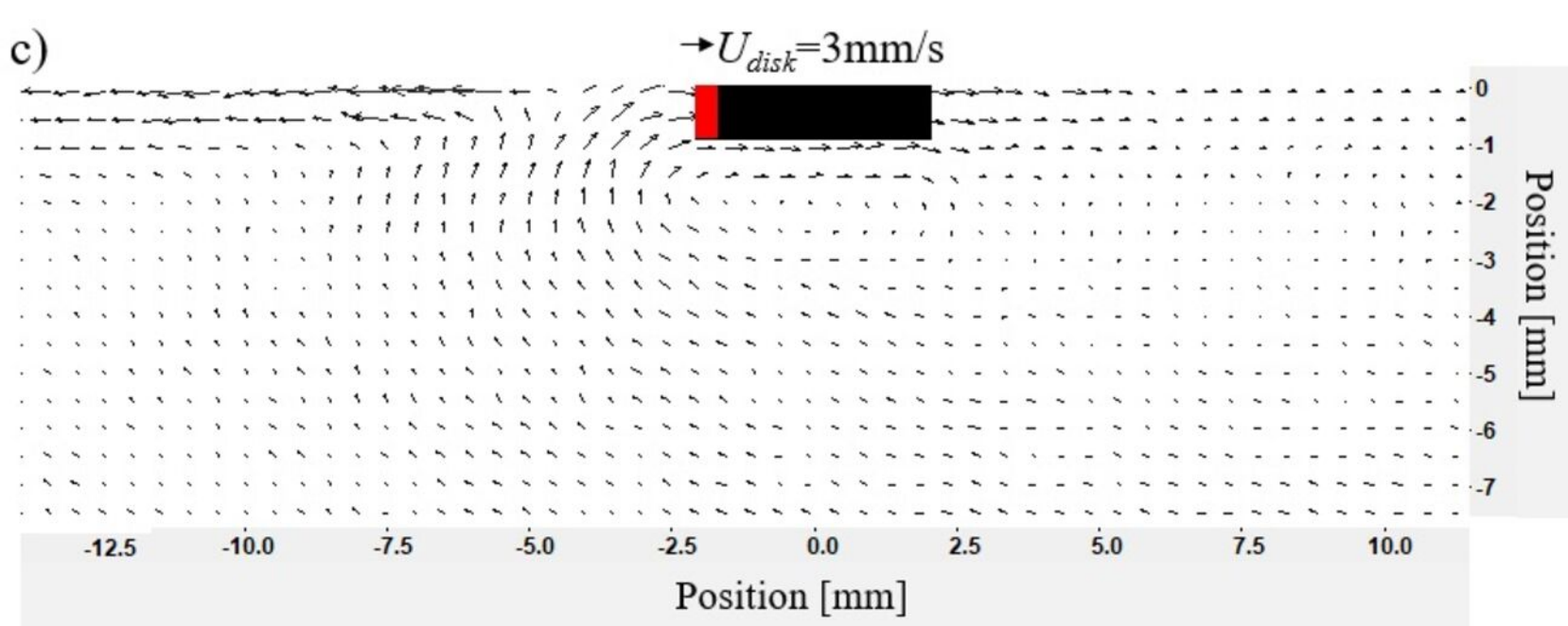
c)
U_{disk}=3mm/s
0
-1
-2
-3
-4
-5
-6
-7
Position [mm]
-12.5
-10.0
-7.5
-5.0
-2.5
0.0
2.5
5.0
7.5
10.0
Position [mm]

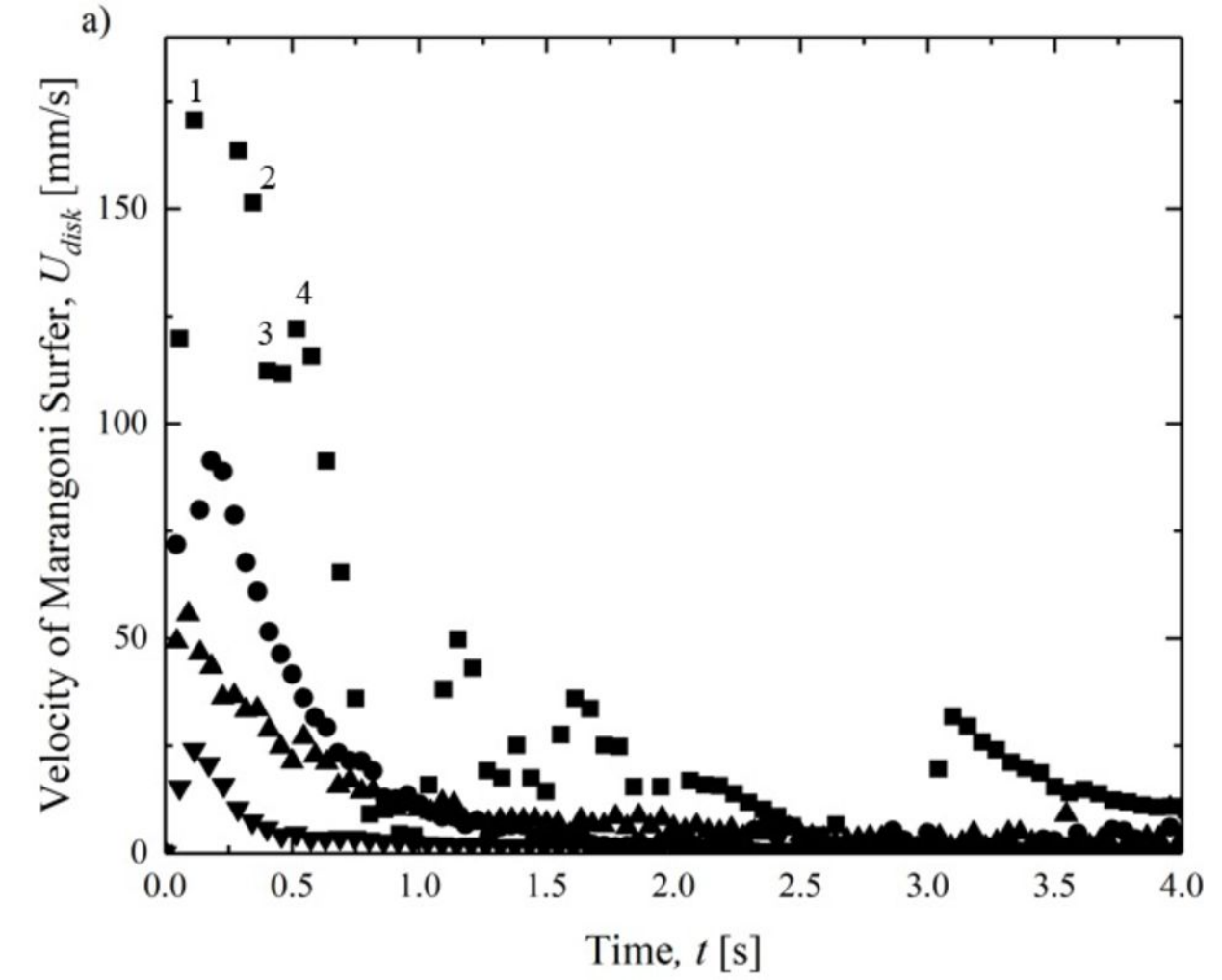
a)
1
2
3
4
Velocity of Marangoni Surfer, U_{disk} [mm/s]
0
50
100
150
0.0
0.5
1.0
1.5
2.0
2.5
3.0
3.5
4.0
Time, t [s]

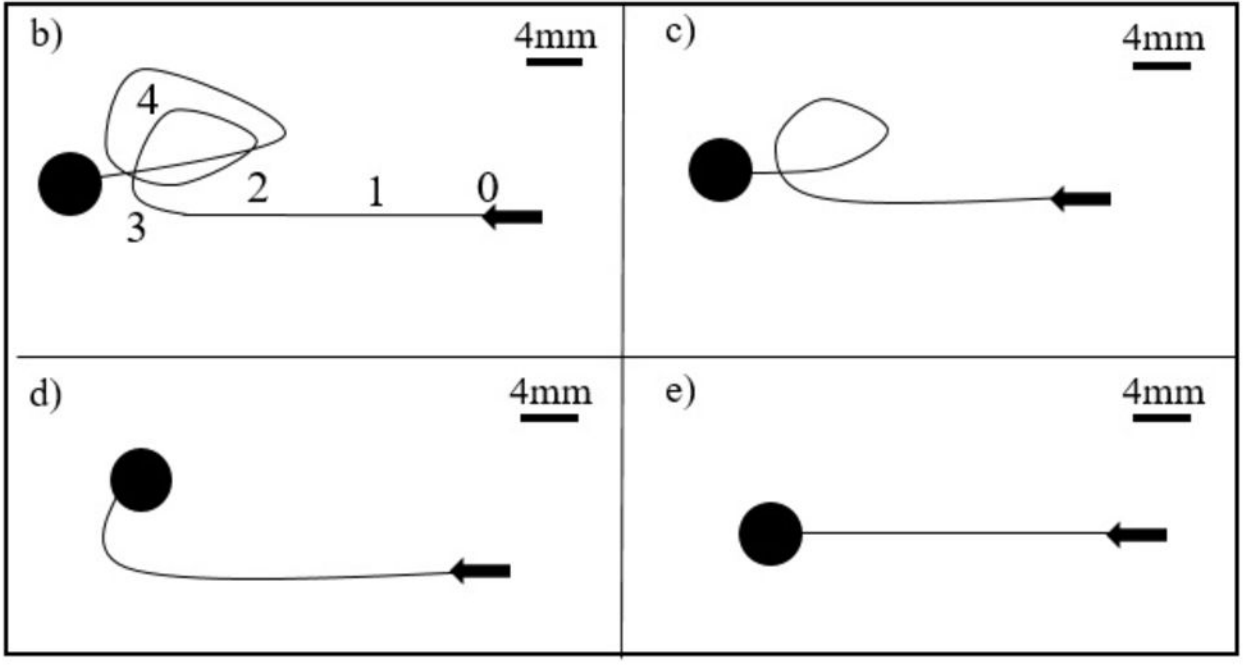
b)
4mm
4
2
1
0
3
c)
4mm
d)
4mm
e)
4mm

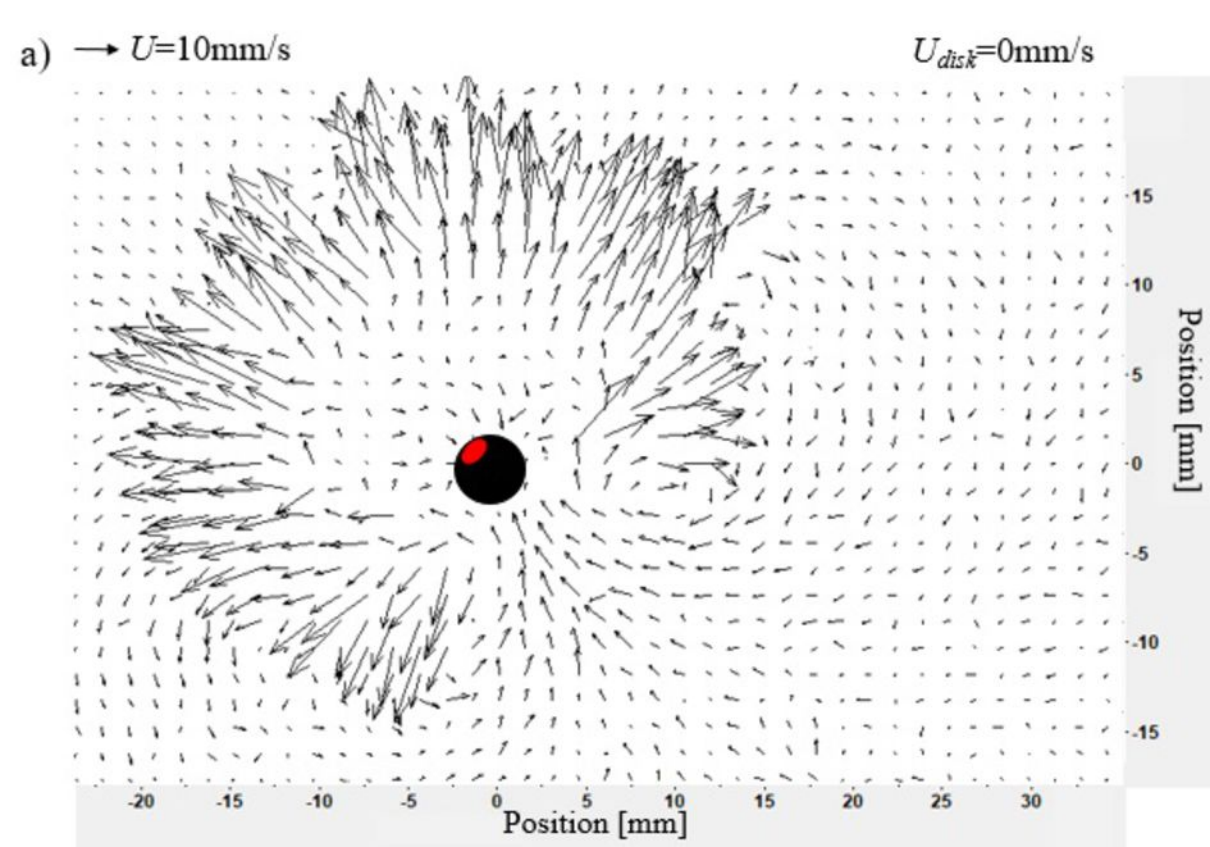
a)
U=10mm/s
U_disk=0mm/s
15
10
5
0
-5
-10
-15
Position [mm]
-20
-15
-10
-5
0
5
10
15
20
25
30
Position [mm]

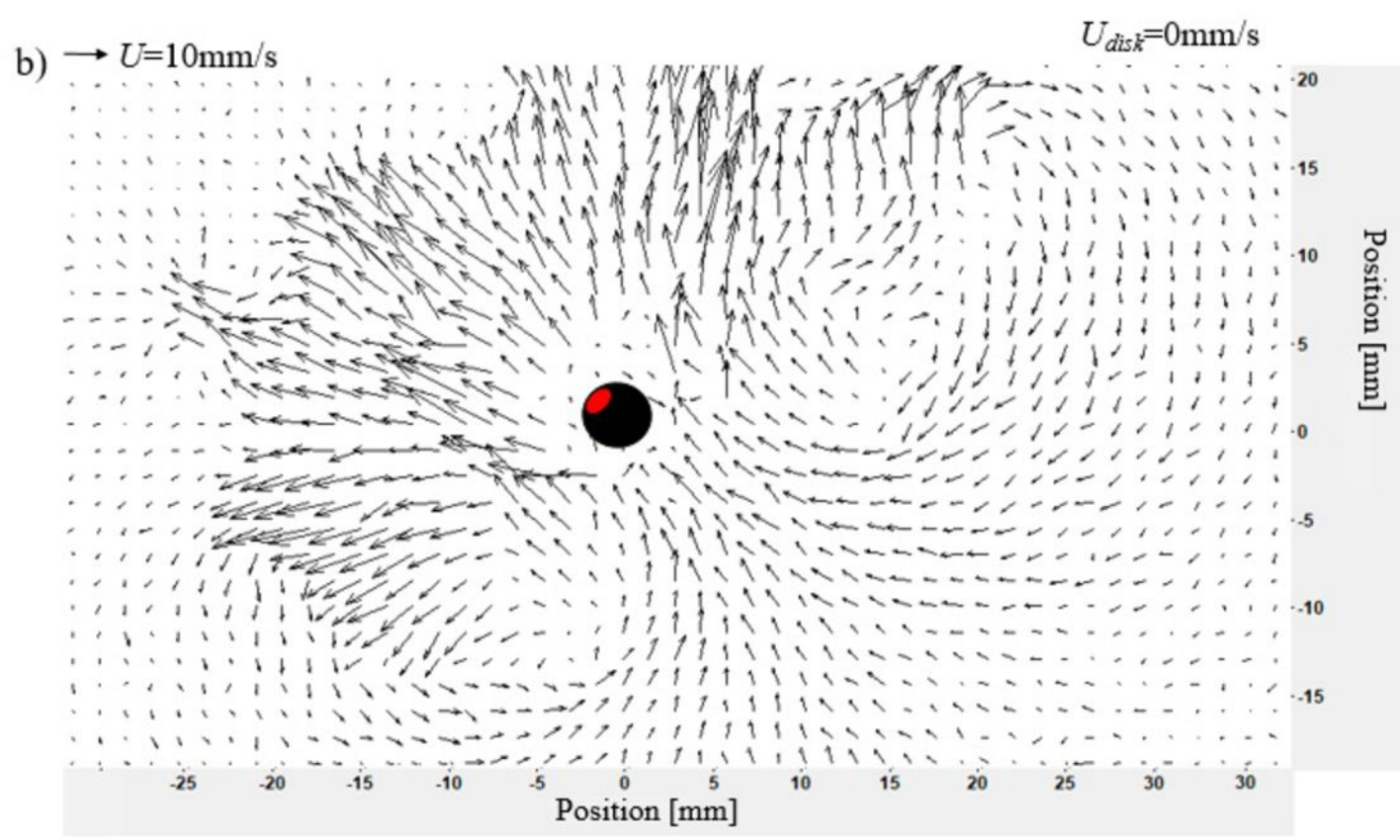
b)
U=10mm/s
U_disk=0mm/s
20
15
10
5
0
-5
-10
-15
Position [mm]
-25
-20
-15
-10
-5
0
5
10
15
20
25
30
30
Position [mm]

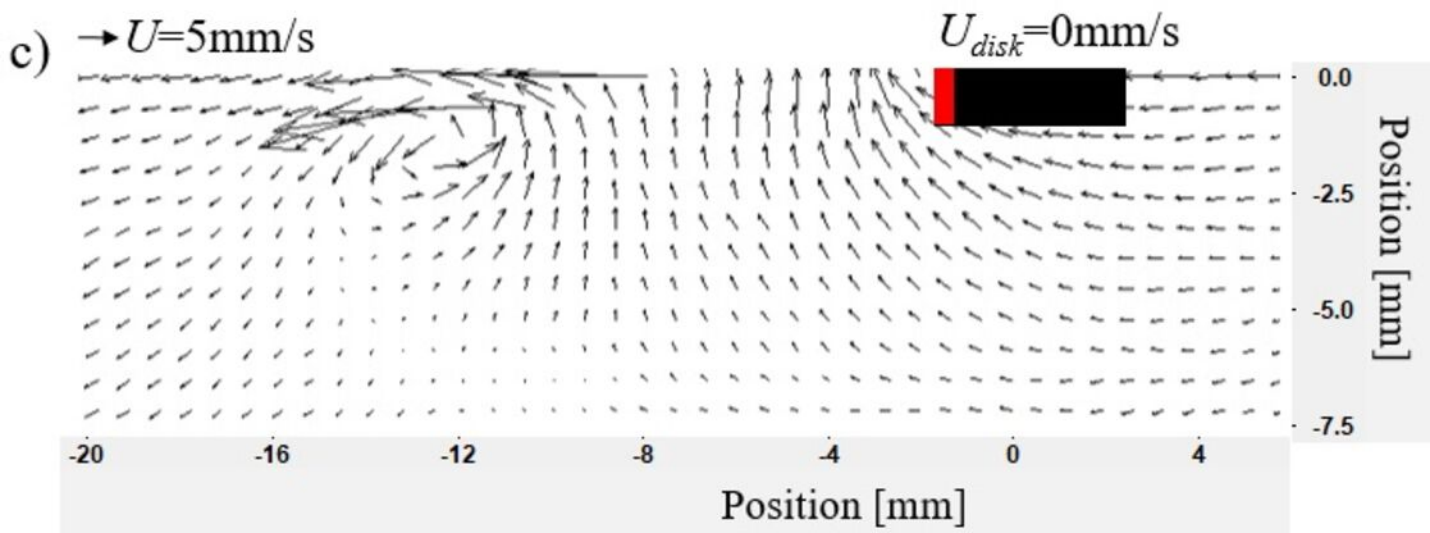
c)
→ U=5mm/s
U_disk=0mm/s
0.0
-2.5
-5.0
-7.5
Position [mm]
-20
-16
-12
-8
-4
0
4
Position [mm]

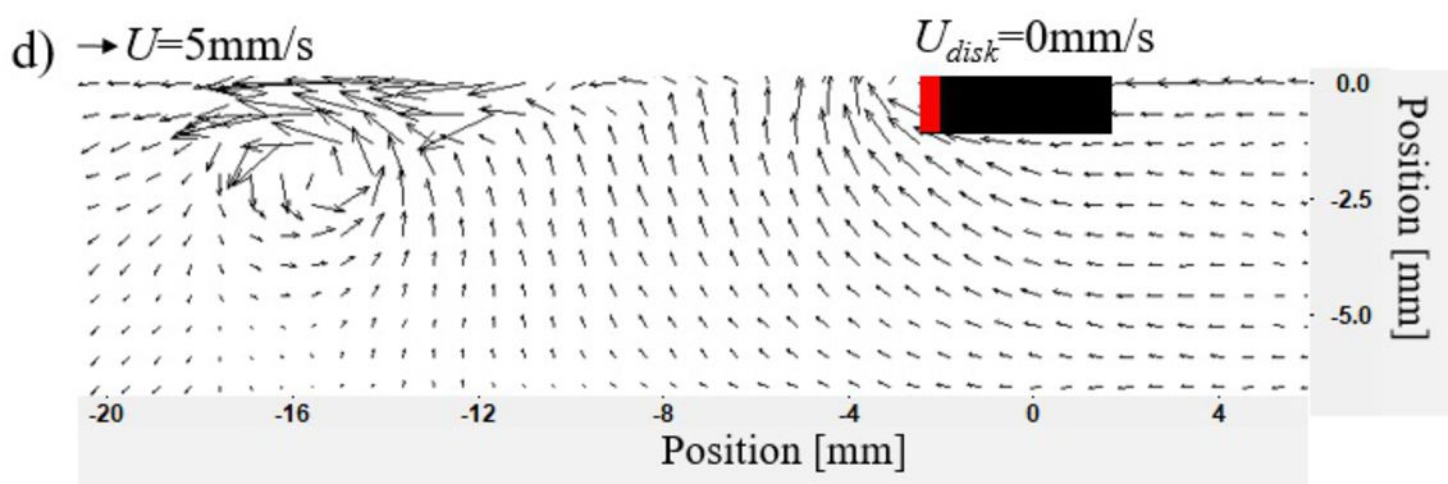
d)
→U=5mm/s
U_disk=0mm/s
0.0
-2.5
-5.0
Position [mm]
-20
-16
-12
-8
-4
0
4
Position [mm]

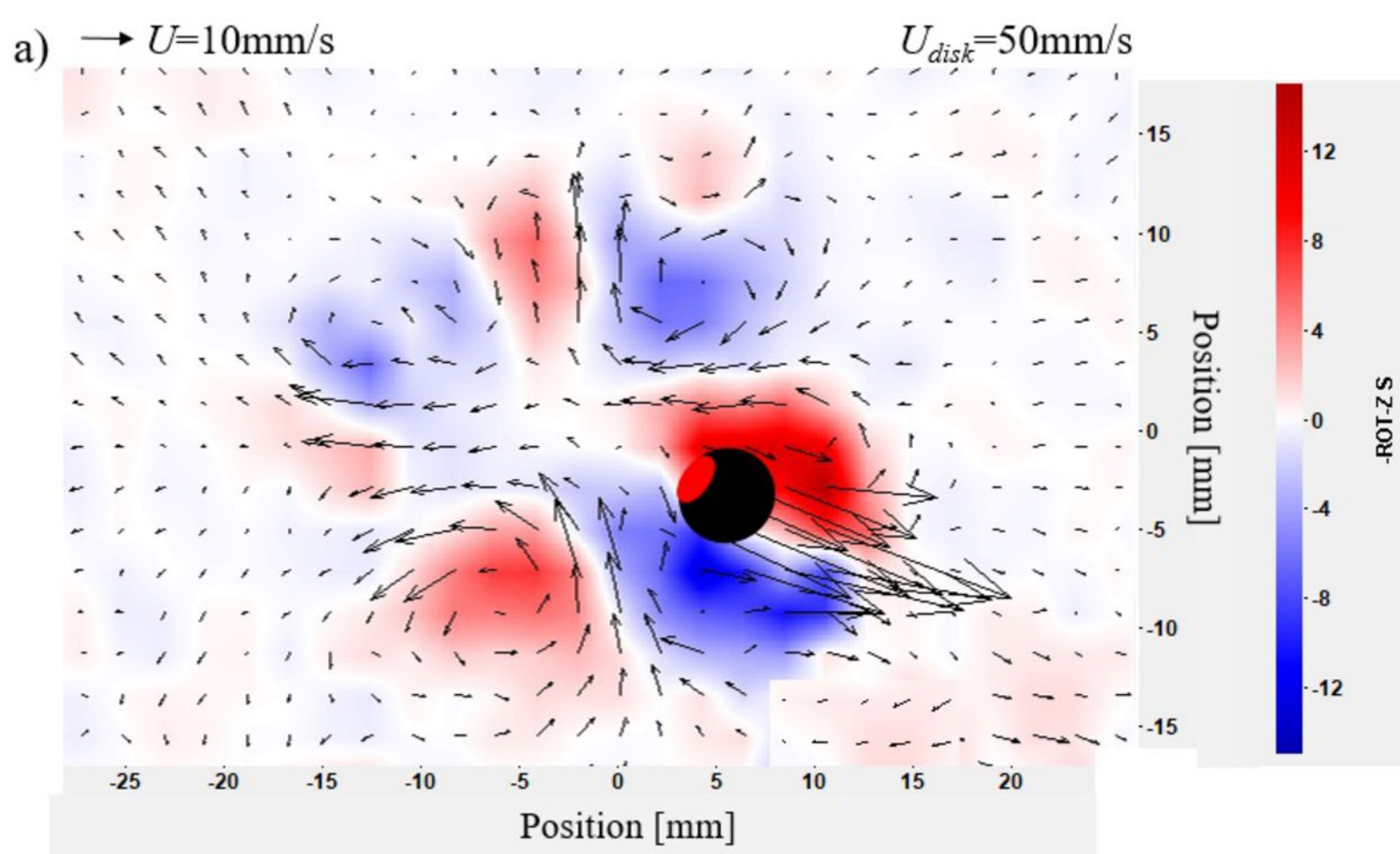
a)
U=10mm/s
U_disk=50mm/s
Position [mm]
Position [mm]
-ROT-Z S
15
10
5
0
-5
-10
-15
-25
-20
-15
-10
-5
0
5
10
15
20
12
8
4
0
-4
-8
-12

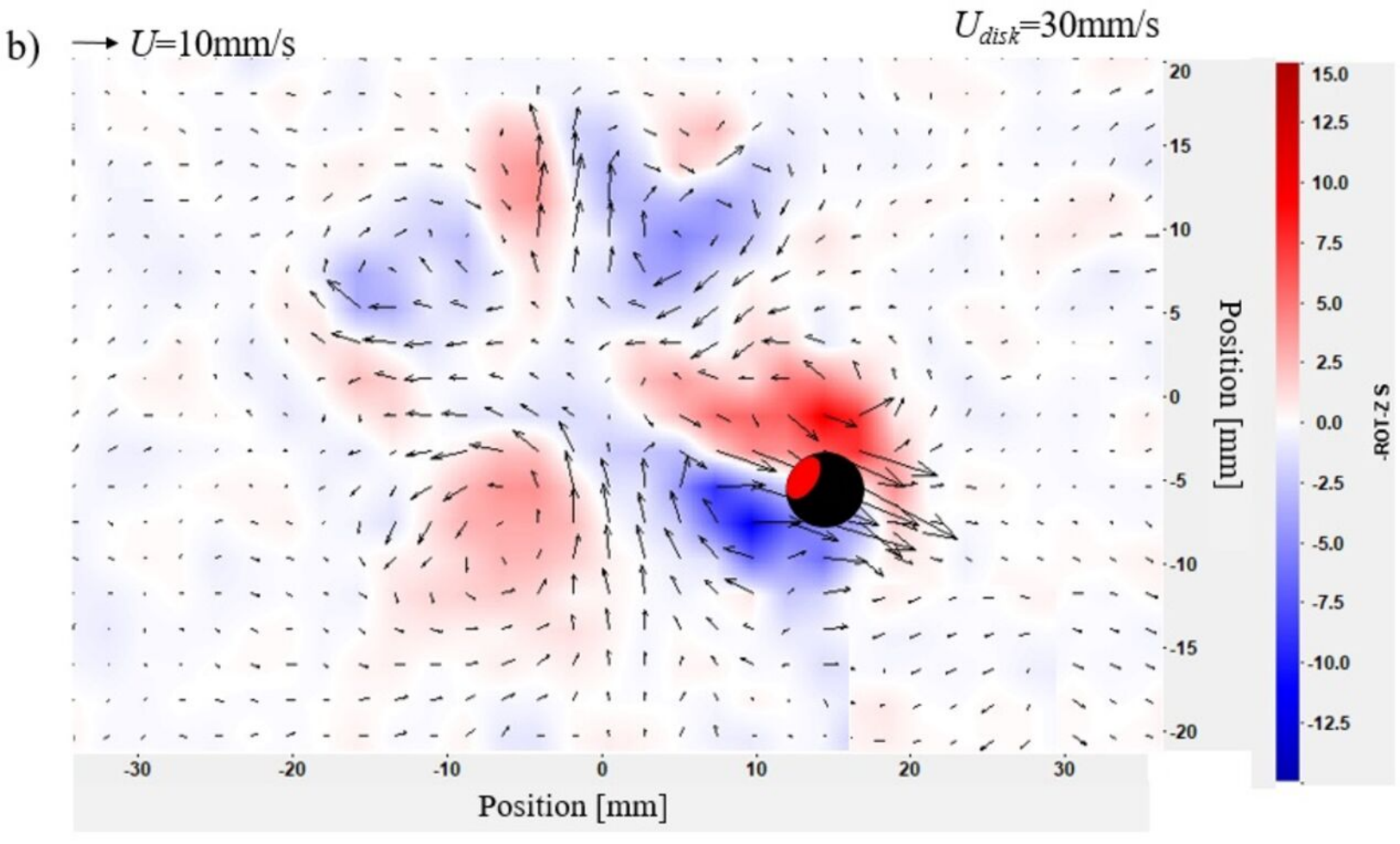
b)
U=10mm/s
U_disk=30mm/s
Position [mm]
Position [mm]
S Z-ROT
15.0
12.5
10.0
7.5
5.0
2.5
0.0
-2.5
-5.0
-7.5
-10.0
-12.5
20
15
10
5
0
-5
-10
-15
-20
-30
-20
-10
0
10
20
30

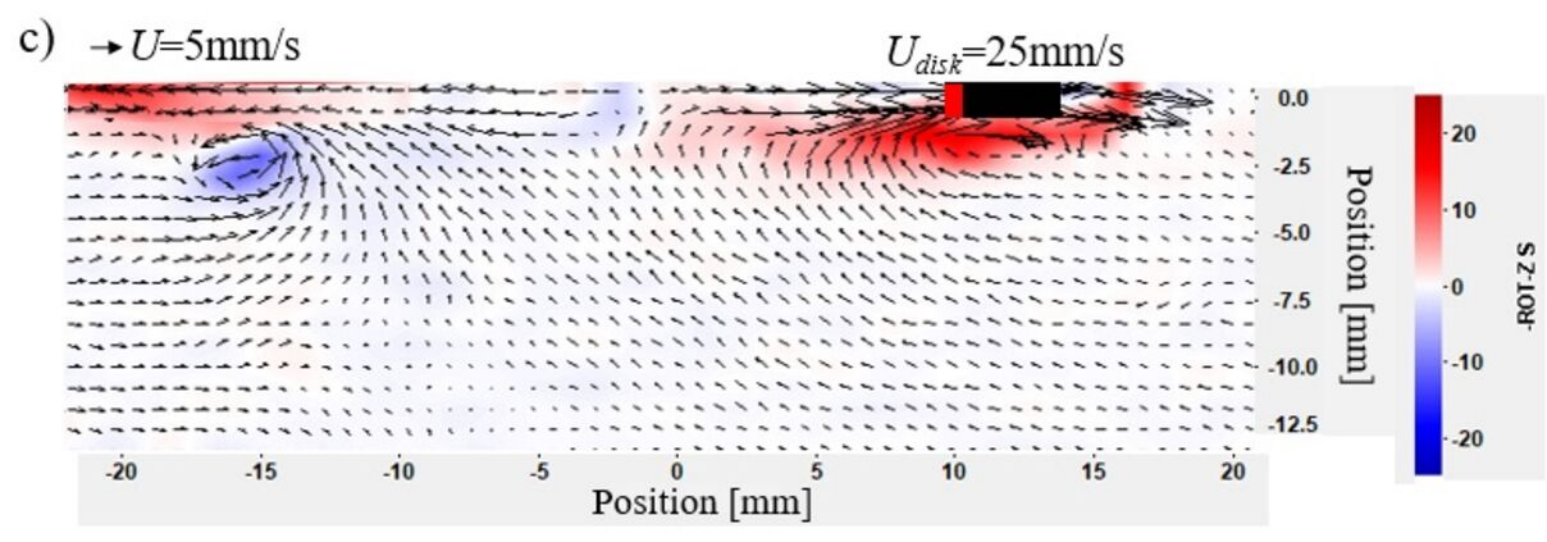
c)
U=5mm/s
U_disk=25mm/s
0.0
-2.5
-5.0
-7.5
-10.0
-12.5
Position [mm]
20
10
0
-10
-20
S_Z-ROT
-20
-15
-10
-5
0
5
10
15
20
Position [mm]

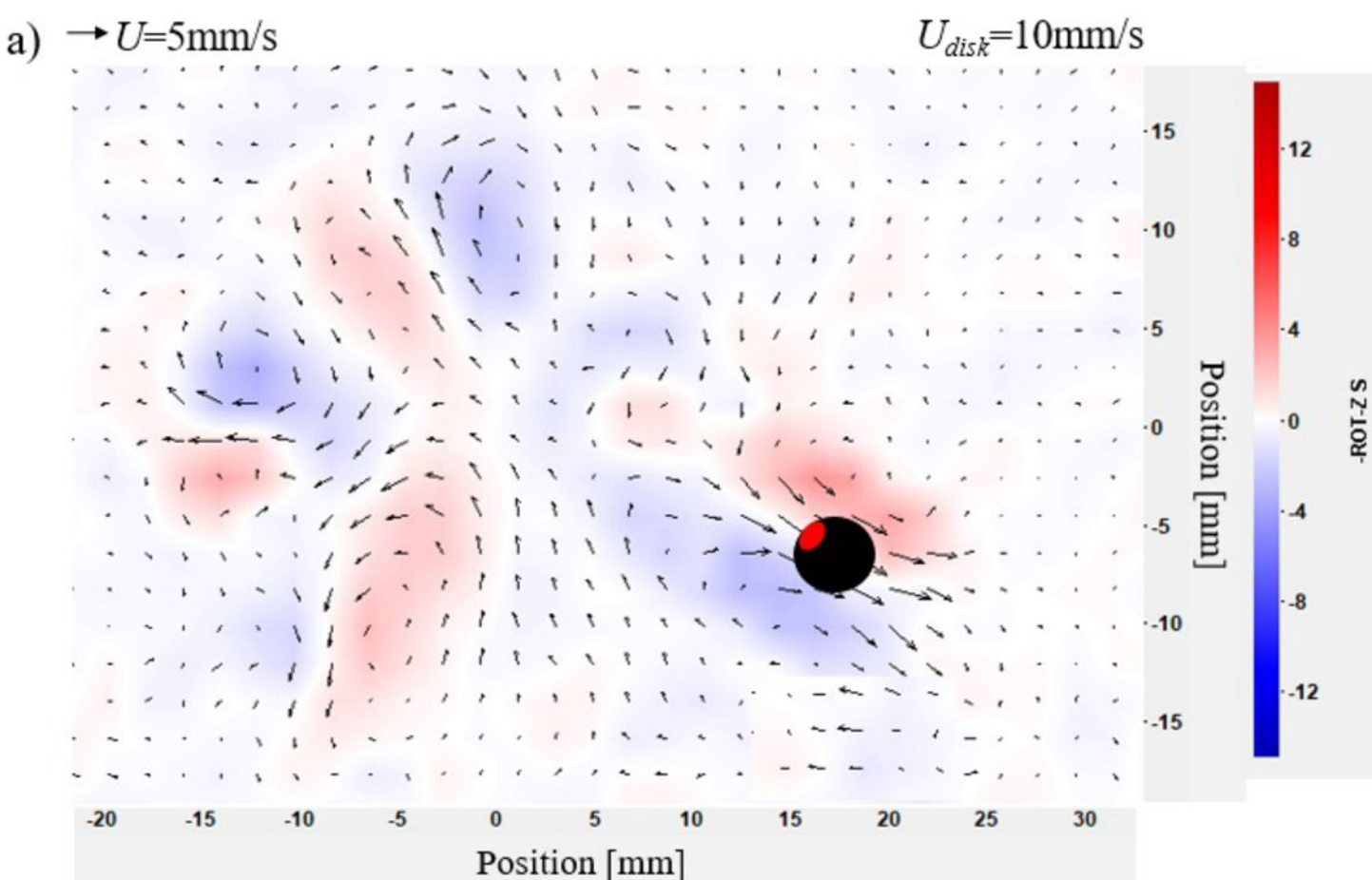
a)
U=5mm/s
U_disk=10mm/s
Position [mm]
Position [mm]
S-Z-ROT

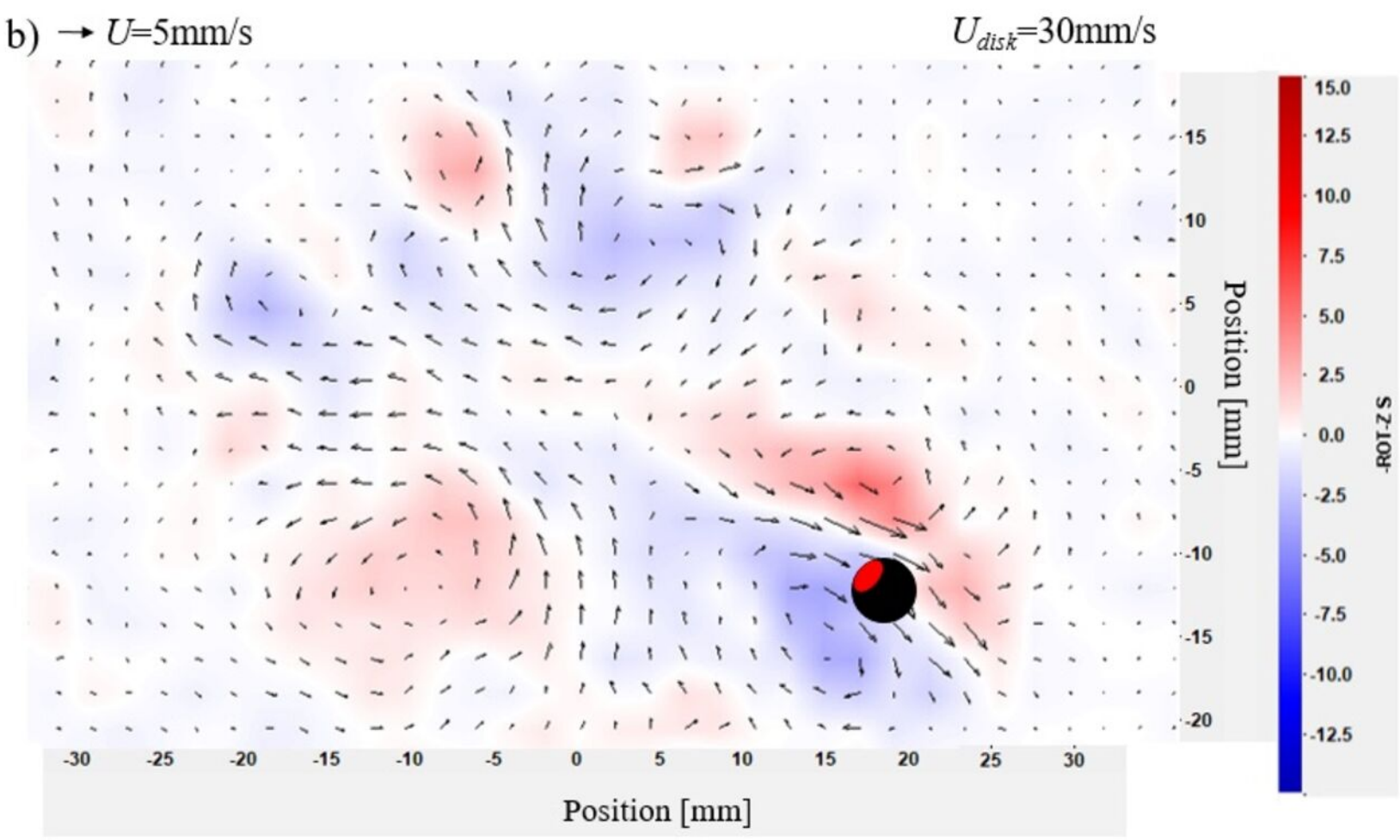
b) → U=5mm/s
U_disk=30mm/s
15
10
5
0
-5
-10
-15
-20
Position [mm]
15.0
12.5
10.0
7.5
5.0
2.5
0.0
-2.5
-5.0
-7.5
-10.0
-12.5
S_Z-10R-
-30
-25
-20
-15
-10
-5
0
5
10
15
20
25
30
Position [mm]

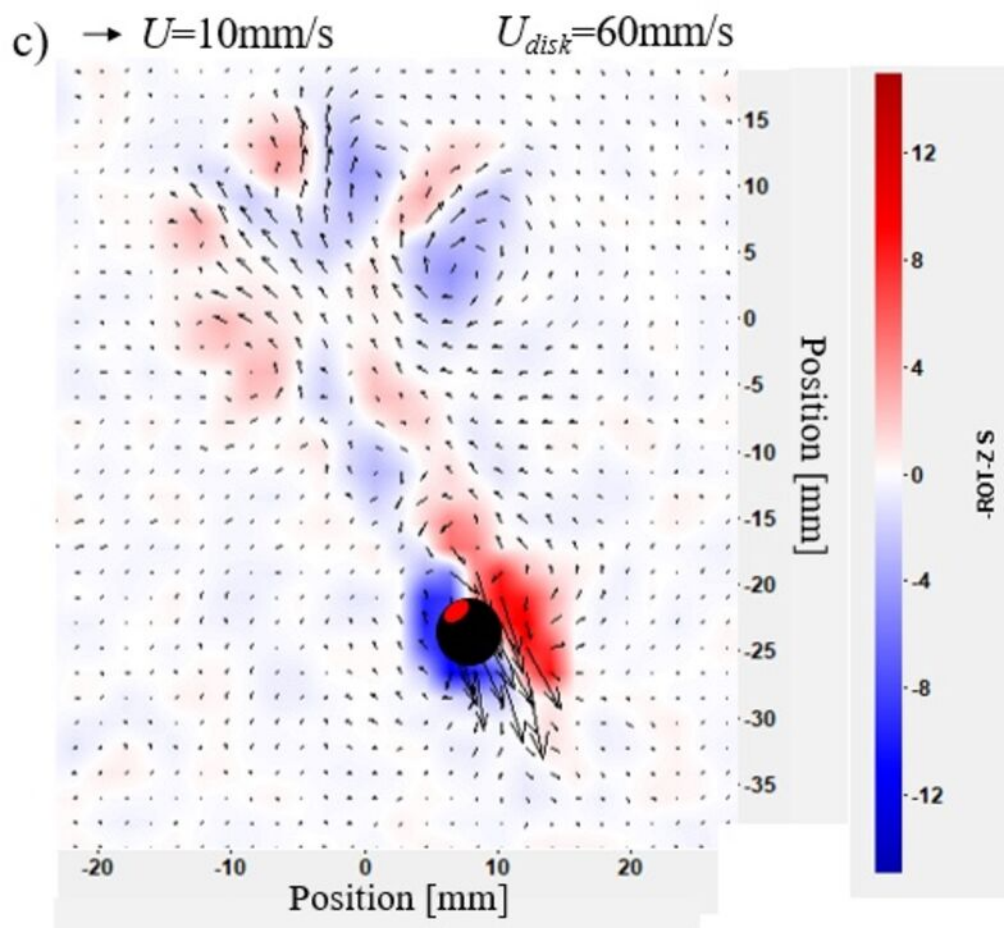
c)
U=10mm/s
U_{disk}=60mm/s
15
10
5
0
-5
-10
-15
-20
-25
-30
-35
Position [mm]
12
8
4
0
-4
-8
-12
S Z-ROT
-20
-10
0
10
20
Position [mm]

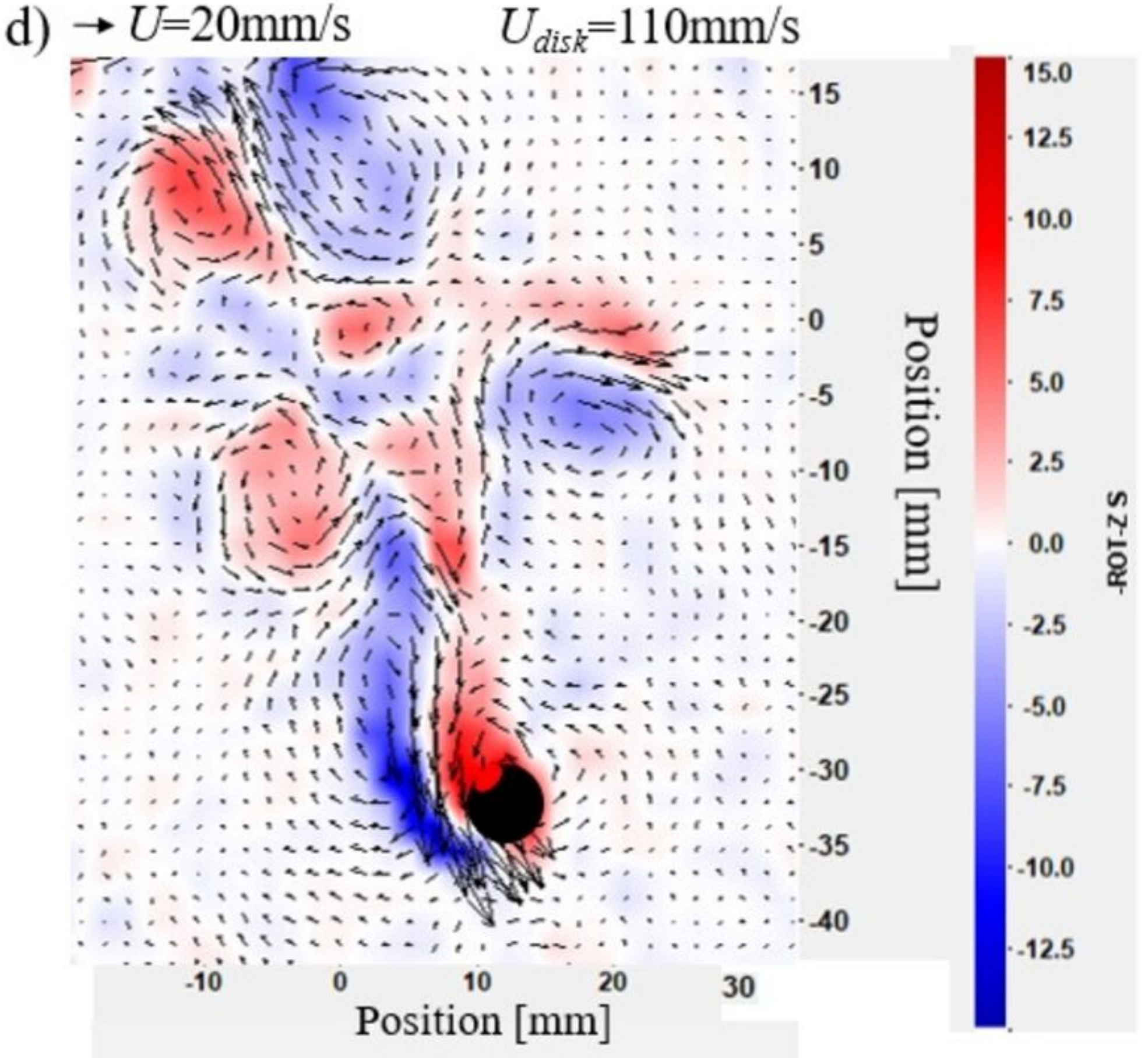
d) → U=20mm/s
U_{disk}=110mm/s
15
10
5
0
-5
-10
-15
-20
-25
-30
-35
-40
Position [mm]
-10
0
10
20
30
Position [mm]
15.0
12.5
10.0
7.5
5.0
2.5
0.0
-2.5
-5.0
-7.5
-10.0
-12.5
-ROT-Z S

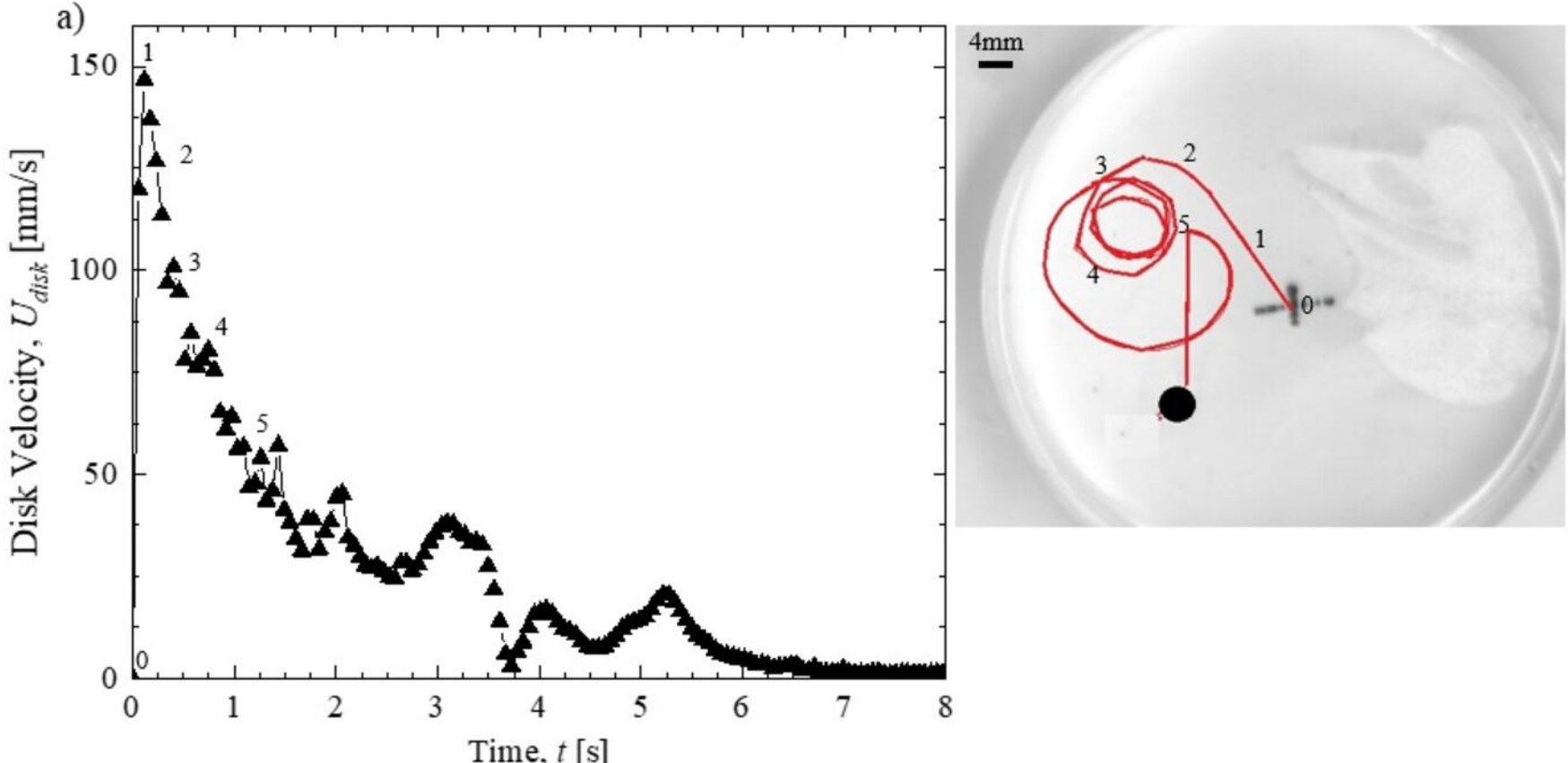
a)
Disk Velocity, U_{disk} [mm/s]
Time, t [s]
0
50
100
150
0
1
2
3
4
5
6
7
8
0
1
2
3
4
5
4mm
0
1
2
3
4
5

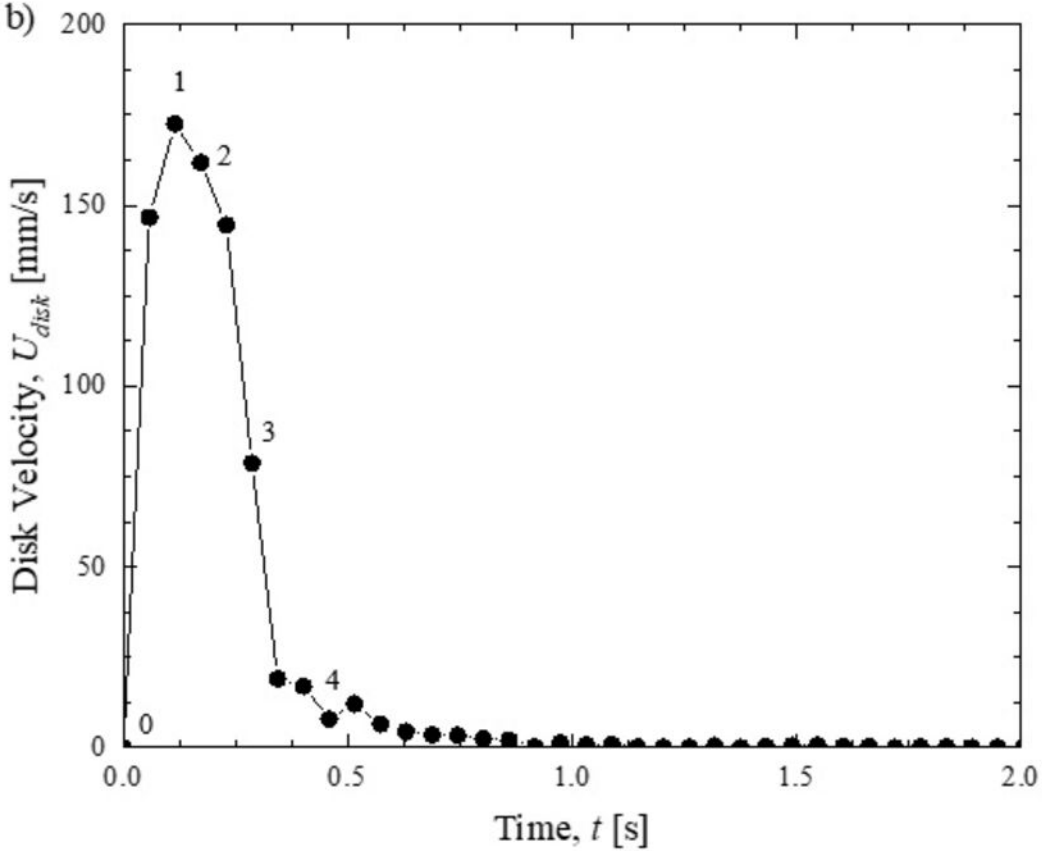
b)
Disk Velocity, U_{disk} [mm/s]
Time, t [s]
0
50
100
150
200
0.0
0.5
1.0
1.5
2.0
0
1
2
3
4

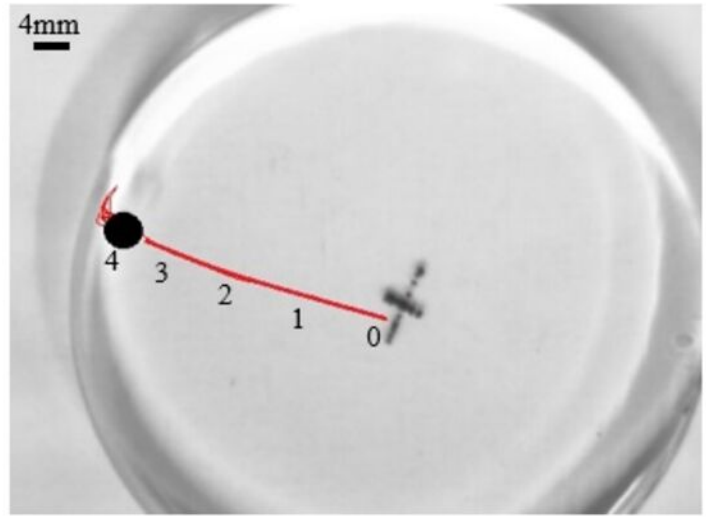
4mm
4
3
2
1
0

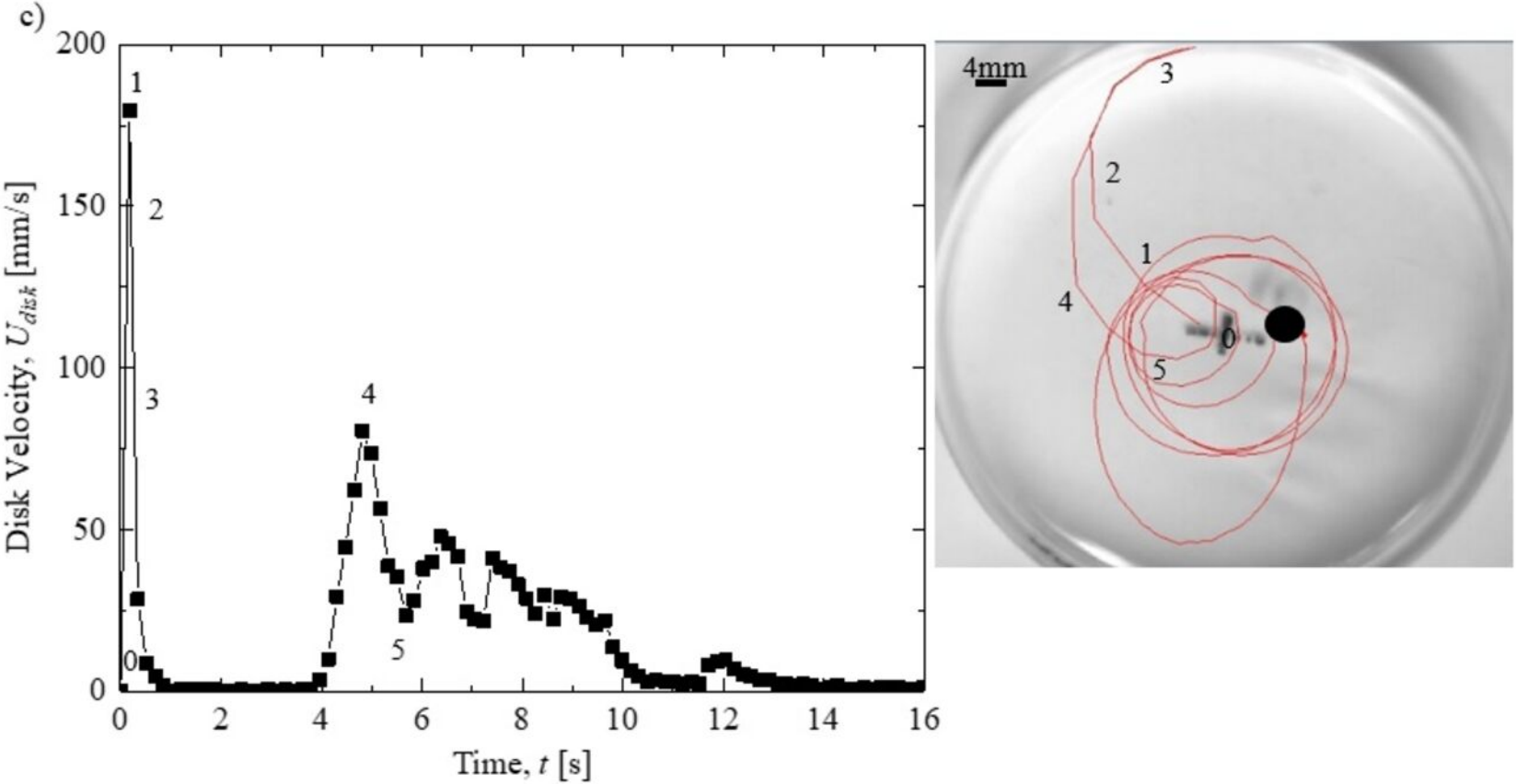
c)
Disk Velocity, U_{disk} [mm/s]
Time, t [s]
0
50
100
150
200
0
2
4
6
8
10
12
14
16
0
1
2
3
4
5
4mm